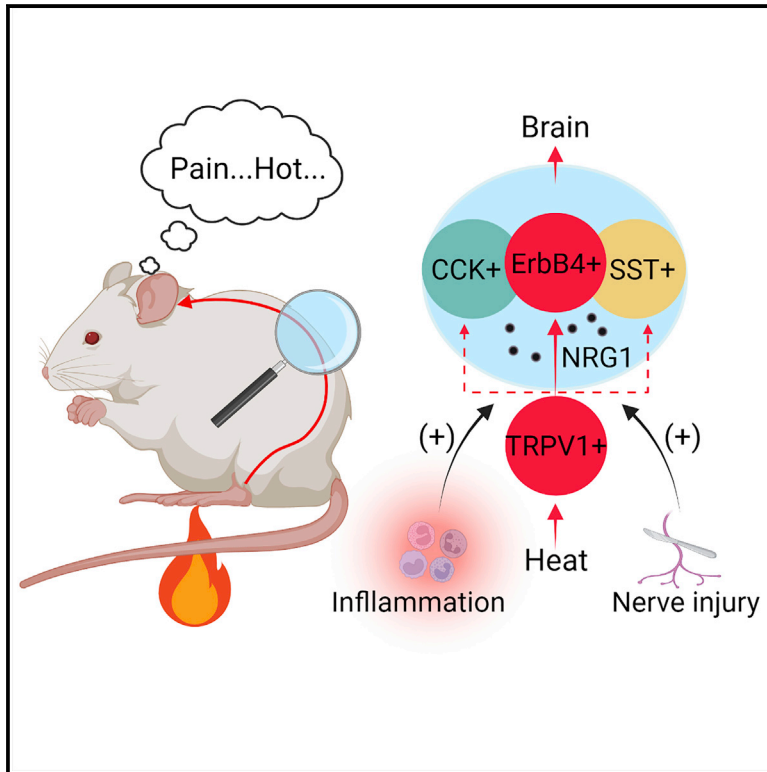


## A novel spinal neuron connection for heat sensation

## Graphical abstract



## Authors

Hongsheng Wang, Wenbing Chen, Zhaoqi Dong, ..., James Meixiong, Wen-Cheng Xiong, Lin Mei

## Correspondence

lin.mei@case.edu

## In brief

How heat signals are processed in the spinal cord remains unclear. Wang et al. found that ErbB4+ excitatory interneurons are activated by noxious heat, and they participate in heat sensation in mice. In addition, the neuregulin-ErbB4 signaling regulates heat sensation and contributes to heat hypersensitivity under pathological conditions.

## Highlights

- Spinal ErbB4+ neurons are activated by heat and synapsed by TRPV1+ nociceptors
- Heat sensation is reduced by ErbB4+ neuron ablation or inhibition
- Augmented effect on heat sensation by inhibiting ErbB4+, SST+, and CCK+ neurons together
- NRG1-ErbB4 signaling promotes heat sensation and hypersensitivity



## Article

# A novel spinal neuron connection for heat sensation

Hongsheng Wang,<sup>1,4</sup> Wenbing Chen,<sup>1,4</sup> Zhaoqi Dong,<sup>1,4</sup> Guanglin Xing,<sup>1</sup> Wanpeng Cui,<sup>1</sup> Lingling Yao,<sup>1</sup> Wen-Jun Zou,<sup>1</sup> Heath L. Robinson,<sup>1</sup> Yaoyao Bian,<sup>1</sup> Zhipeng Liu,<sup>1</sup> Kai Zhao,<sup>1</sup> Bin Luo,<sup>1</sup> Nannan Gao,<sup>1</sup> Hongsheng Zhang,<sup>1</sup> Xiao Ren,<sup>1</sup> Zheng Yu,<sup>1</sup> James Meixiong,<sup>3</sup> Wen-Cheng Xiong,<sup>1,2</sup> and Lin Mei<sup>1,2,5,\*</sup>

<sup>1</sup>Department of Neurosciences, School of Medicine, Case Western Reserve University, 10900 Euclid Avenue, Cleveland, OH 44106, USA

<sup>2</sup>Louis Stokes Cleveland Veterans Affairs Medical Center, Cleveland, OH 44106, USA

<sup>3</sup>Solomon H. Snyder Department of Neuroscience and Medical Scientist Training Program, Johns Hopkins University School of Medicine, Baltimore, MD 21205, USA

<sup>4</sup>These authors contributed equally

<sup>5</sup>Lead contact

\*Correspondence: [lin.mei@case.edu](mailto:lin.mei@case.edu)

<https://doi.org/10.1016/j.neuron.2022.04.021>

## SUMMARY

Heat perception enables acute avoidance responses to prevent tissue damage and maintain body thermal homeostasis. Unlike other modalities, how heat signals are processed in the spinal cord remains unclear. By single-cell gene profiling, we identified ErbB4, a transmembrane tyrosine kinase, as a novel marker of heat-sensitive spinal neurons in mice. Ablating spinal ErbB4<sup>+</sup> neurons attenuates heat sensation. These neurons receive monosynaptic inputs from TRPV1<sup>+</sup> nociceptors and form excitatory synapses onto target neurons. Activation of ErbB4<sup>+</sup> neurons enhances the heat response, while inhibition reduces the heat response. We showed that heat sensation is regulated by NRG1, an activator of ErbB4, and it involves dynamic activity of the tyrosine kinase that promotes glutamatergic transmission. Evidence indicates that the NRG1-ErbB4 signaling is also engaged in hypereosensitivity of pathological pain. Together, these results identify a spinal neuron connection consisting of ErbB4<sup>+</sup> neurons for heat sensation and reveal a regulatory mechanism by the NRG1-ErbB4 signaling.

## INTRODUCTION

Long exposure to noxious heat causes tissue damage and disrupts the homeostasis of body temperature. In human, skin temperature above 43°C evokes acute pain (Basbaum et al., 2009; Vriens et al., 2014), and exposure to a temperature as low as 44°C causes cutaneous burn injury (Moritz and Henriques, 1947). Heat sensation enables acute avoidance responses to prevent tissue damage and maintain body thermal homeostasis. Heat sensitivity is increased in diseases such as systemic inflammatory disorders, peripheral nerve injuries, chemotherapy-induced neuropathy, and postherpetic neuralgia (Colloca et al., 2017). Noxious heat is sensed by dorsal root ganglion (DRG) neurons expressing the transient receptor potential family member V1 (TRPV1) channel (Caterina et al., 1997; Tominaga et al., 1998). Elimination or inactivation of TRPV1<sup>+</sup> DRG neurons in mice diminishes the sensation of noxious heat (Brenneis et al., 2013; Cavanaugh et al., 2009; Pogorzala et al., 2013).

Interneurons (INs) in the dorsal horn are critical in processing and relaying sensory signals from afferent fibers of DRG nociceptors (Basbaum et al., 2009; Todd, 2010). They are different in morphology, electrophysiological properties, gene expression profiles, and location. Such complex diversity serves as a good

substrate for encoding of different somatosensory modalities (Gradwell and Abaira, 2021; Koch et al., 2018; Peirs and Seal, 2016; Prescott et al., 2014; Todd, 2010). There are two major theories for somatosensory information processing (Craig, 2003; Ma, 2010; Moayedi and Davis, 2013; Perl, 2007). In the labeled line hypothesis, sensory information in response to individual stimuli could be processed by specific neuronal circuits or labeled lines that transmit the signal from sensory organs to the brain (Andrew and Craig, 2001; Blix, 1882; Cavanaugh et al., 2009; Duan et al., 2014; Emery et al., 2016; Hachisuka et al., 2020; Müller, 1840; Norrsell et al., 1999). In support of the labeled line model are that ablation of TRPV1<sup>+</sup>, TRPM8<sup>+</sup>, MAS-related GPR family member D-expressive (MrgprD<sup>+</sup>), and MrgprA3<sup>+</sup> DRG neurons impairs noxious heat, cold, mechanical and itch sensation, respectively (Cavanaugh et al., 2009; Han et al., 2013; Knowlton et al., 2013). In addition, behavioral responses to modalities like chemical itch, mechanical itch, and mechanical pain are abolished by ablating or inhibiting a group of spinal INs (Duan et al., 2014; Pan et al., 2019; Sun et al., 2009). On the other hand, the population-coding model (also referred to as pattern theory) proposes that a modality could be processed by joint activities of different types of neurons (Abaira et al., 2017; Arcourt et al., 2017; Craig and Bushnell,



1994; Gatto et al., 2021; McCoy et al., 2013; Paricio-Montesinos et al., 2020; Thunberg, 1896). In support of the latter model are the phenomenon of thermal grill illusion and gate control theory (Green, 2004; Melzack and Wall, 1965). Neurons in the DRG and superficial layers of the spinal cord are usually polymodal (Han et al., 1998; Paricio-Montesinos et al., 2020; Sharif et al., 2020; Wang et al., 2018a); more recently, heat stimulation was shown to increase cFos or Arc expression in different populations of spinal INs (Håring et al., 2018; Polgár et al., 2013). In addition, warm perception or reflexive responses to chloroquine or mechanical stimuli have been shown to involve heterogeneous populations of molecularly defined neurons that are functionally independent (Arcourt et al., 2017; Fatima et al., 2019; Gatto et al., 2021; Paricio-Montesinos et al., 2020). However, neurons that process heat signals in the spinal cord remain unclear. Nevertheless, developmental deletion of transcriptional factors, including *Hoxb8*, *Pbx3*, *Imx1b*, *Tlx3*, or *TR4* results in neuronal loss in the superficial layers and diminishes the response to heat as well as mechanical, cold, and pruritogenic stimuli (Holstege et al., 2008; Rottkamp et al., 2008; Szabo et al., 2015; Wang et al., 2013; Xu et al., 2013). The identity of heat-processing neurons in the spinal cord is yet to be revealed. For example, data were inconsistent regarding the role of somatostatin+ (SST+) neurons in heat sensation (Christensen et al., 2016; Duan et al., 2014); ablating cholecystokinin+ (CCK+) neurons had little effect on heat reflexes (Liu et al., 2018; Wercberger et al., 2021).

Here, we show that diverse INs in the spinal cord were activated by noxious heat, each group (such as SST+ or CCK+ neurons) accounting for a minor fraction of the total cFos+ population. However, a significant portion of cFos+ neurons expressed ErbB4, which is a receptor tyrosine kinase of the epidermal growth factor receptor (EGFR) family that is activated by the growth factor neuregulin 1 (NRG1), identifying a novel marker of spinal neurons and providing a handle to investigate heat sensation in the dorsal horn. Ablating ErbB4+ neurons in the spinal dorsal horn attenuated the acute response to noxious heat; their activation and inhibition enhanced and suppressed, respectively, heat sensation. Interestingly, simultaneous ablation or inhibition of spinal ErbB4+, SST+, and CCK+ neurons caused a more prominent inhibitory effect, in support of the population-coding model for heat information processing. We characterized DRG afferent inputs to ErbB4+ neurons and their responses to heat stimuli. Considering that NRG1-ErbB4 signaling is critical to GABAergic transmission in the brain (Mei and Nave, 2014), we investigated its involvement in heat sensation and potential contribution to heat hypersensitivity under pathological conditions. Our results indicate that ErbB4+ INs are innervated by TRPV1+ nociceptors, and they respond to noxious heat and form excitatory synapses onto downstream spinal neurons. This local neuron connection is involved in noxious heat sensation and is regulated by the NRG1-ErbB4 signaling.

## RESULTS

### Activation of ErbB4+ excitatory neurons by noxious heat

To identify neurons that respond to noxious heat, we took advantage of cFos::shEGFP mice that express a short half-life EGFP

(shEGFP) under the control of endogenous cFos promoter (Figure 1A) (Reijmers et al., 2007). shEGFP expression is increased by neuronal activity (Du et al., 2017; Ramirez et al., 2013). When cFos::shEGFP mice were subjected to noxious heat (52°C hot plate), shEGFP expression was increased in neurons of spinal cord dorsal horns (Figures 1B and 1C), compared with mice exposed to 25°C plate, in agreement with early findings (Cavanaugh et al., 2009; Hunt et al., 1987). A large number of shEGFP+ neurons were localized in superficial layers (laminae I and II) (Figures 1B and 1C), which are recipient zones for noxious somatosensory information (Light and Perl, 1979; Todd, 2010). shEGFP+ neurons in deep layers (laminae III–V) were not increased in the 52°C group, compared with the 25°C group (Figures 1B and 1C). cFos revealed by anti-cFos antibody overlapped with that of shEGFP in superficial layers, suggesting shEGFP as a faithful indicator of activated neurons (Figures 1D and 1E). To characterize shEGFP+ neurons, they were isolated individually by glass pipettes and subjected to single-cell RT-PCR (Figure 1F) for a panel of markers (Figure 1G) (Koch et al., 2018). As shown in the Figure 1H, 78% (39/50) of shEGFP+ cells were positive for *Vglut2* (vesicular glutamate transporter 2), a marker of excitatory neurons, whereas 22% (11/50) were positive for *GAD65/67* (glutamate decarboxylase 65/67), markers of GABAergic neurons (Figures 1G and 1H), consistent with previous findings that a majority of neurons responsive to noxious heat are excitatory (Håring et al., 2018). However, shEGFP+ cells were extremely heterogeneous, with each marker labeling a small fraction of shEGFP+ cells (for example, 18% and 14% for CCK+ and SST+, respectively) (Figure 1I). Remarkably, ErbB4 was expressed in a third of shEGFP+ cells (Figure 1J) and was present in 41% of the excitatory neurons (Figure 1K) but was not detectable in GADs+ cells (data not shown). Altogether, these findings indicate that noxious heat stimulates a group of excitatory neurons that are ErbB4+.

To further test this hypothesis, we subjected ErbB4::CreER;Ai9 mice (Figure S1A) to hot plate stimulation, where tdTomato is expressed under the control of endogenous ErbB4 promoter (Madisen et al., 2010), and thus, its expression enables labeling ErbB4+ (i.e., ErbB4-tdT) cells (Bean et al., 2014; Lin et al., 2018; Shamir et al., 2012). In the spinal cord, ErbB4-tdT cells were mostly concentrated in the dorsal horn (Figures S1B–S1D). In accord, ErbB4 was expressed more in the dorsal horn than in the ventral horn (Figure S1E). Within the dorsal horn, ErbB4-tdT cells are present in various layers and the lateral spinal nucleus (LSN) (Figures S1C and S1D). However, heat-induced cFos was mostly in ErbB4-tdT neurons in superficial layers (Figures 1M–1O). ErbB4-tdT neurons accounted for about 33% of cFos+ neurons by noxious heat (Figures 1M and 1N). Together, these results identify ErbB4+ excitatory neurons in the superficial layers as a novel class of noxious heat-responding cells. This notion is supported by analysis of single-nuclei RNA sequencing (snRNA-seq) data where excitatory cells are positive for *Vglut2* (or *Slc7a6* in the database) (Figure S2) (Russ et al., 2021). Of the 21 clusters of *Vglut2*+ cells, ErbB4+ neurons are present in a cluster that is positive for *Nmur2*, a protein enriched in the superficial layer and required for thermal sensation (Zeng et al., 2006).

Morphologically, ErbB4+ neurons in lamina I exhibited longitudinal spindle-shaped soma and bipolar dendritic trees enriched

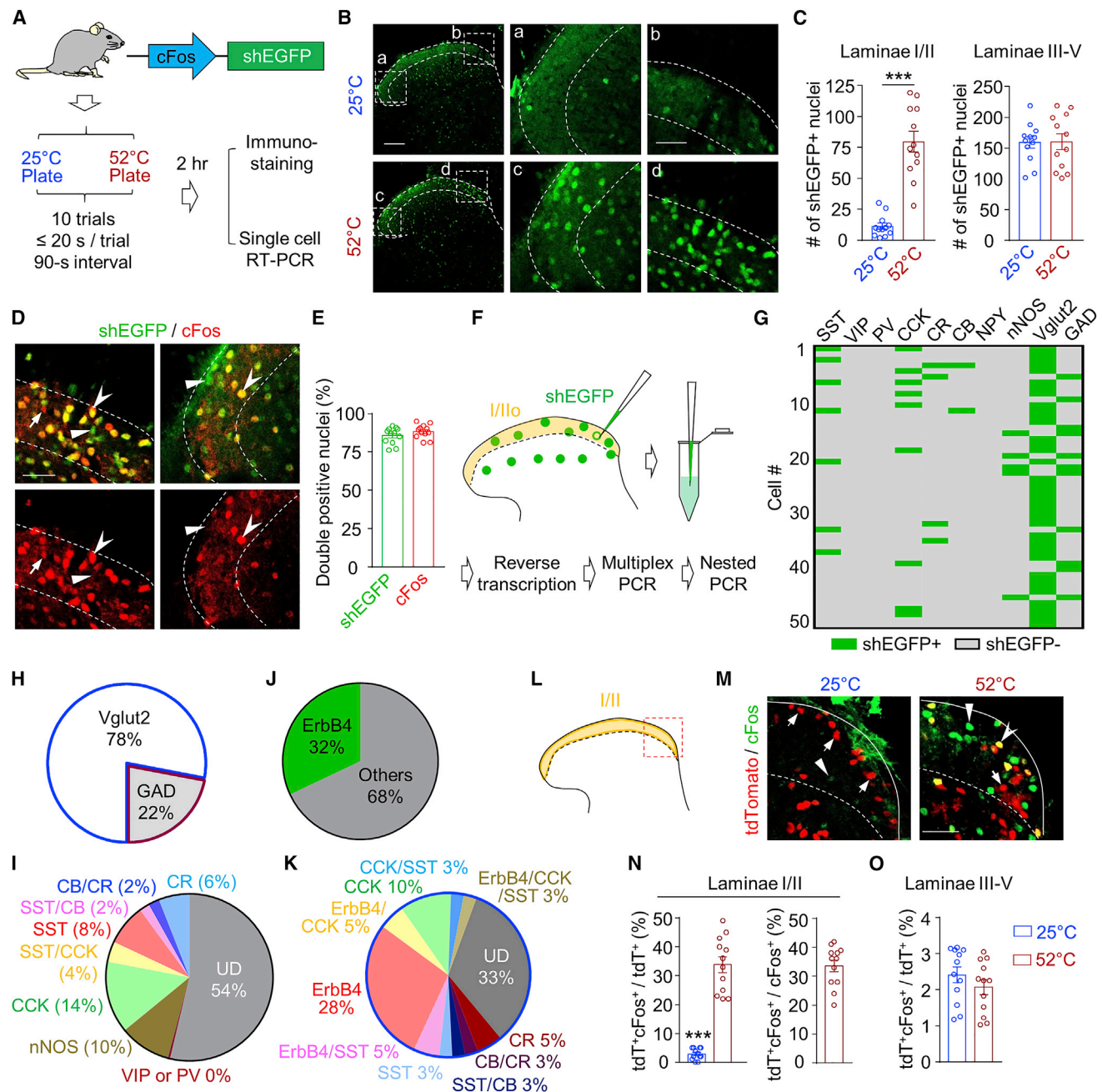


**Figure 1. Activation of ErbB4<sup>+</sup> spinal neurons by noxious heat**

(A) Experimental design.

(B and C) Immunostaining showing increased shEGFP<sup>+</sup> cells in superficial layers (laminae I and II) of the spinal cord after hot plate exposure. (B) Representative images. Left, low-power; scale bar, 100 μm; right, high-power of areas in squares; scale bar, 50 μm. (C) Increased shEGFP<sup>+</sup> cells in superficial layers (left) but not deep layers (laminae III–V, right). t test, \*\*\*p < 0.001; n = 12 slices of 3 mice.

(D and E) Expression of intrinsic cFos in shEGFP<sup>+</sup> cells after 52°C hot plate exposure. (D) Representative images. Arrowheads, shEGFP<sup>+</sup>cFos<sup>+</sup> cells; arrows, shEGFP<sup>-</sup>cFos<sup>+</sup> cells; triangles, shEGFP<sup>+</sup>cFos<sup>-</sup> cells; scale bar, 100 μm. (E) High percentage of double positive of shEGFP<sup>+</sup>cFos<sup>+</sup>.

(F) Diagram showing single-cell RT-PCR strategy.

(G) Gene profiles from 50 shEGFP<sup>+</sup> cells. CR, calretinin, CB, calbindin.

(H) shEGFP<sup>+</sup> cells positive for Vglut2 or GAD65/67.

(I) shEGFP<sup>+</sup> cells positive of reported IN markers.

(legend continued on next page)

with spines (Figures S3A and S3B), which are characteristics of longitudinal fusiform neurons (Lima and Coimbra, 1986), some of which were shown to respond to noxious stimuli (Han et al., 1998). In lamina II, ErbB4+ neurons had dendritic arbors expanding dorsally or in all directions (Figure S3C). Based on firing patterns in response to current injection, ErbB4+ neurons could be classified as “initial burst” (48.7%), delayed firing (35.3%), phasic burst (9.2%), and single-spike firing (6.7%) (Figures S3F and S3G). However, most heat-responsive (i.e., cFos+) ErbB4+ neurons are initial bursting (Figures S3I–S3K), a type that was known to be stimulated by noxious stimuli (Han et al., 1998; Lopez-Garcia and King, 1994). Retrograde tracing by injecting fluorogold into brain regions that are known to be targeted by projection neurons of the spinal cord suggests that ErbB4+ neurons in lamina I/II are predominantly INs, whereas some in deep layers and LSN project to the brain (Figure S4). In agreement, 20%–30% of ErbB4+ neurons in LSN are positive with tachykinin precursor 1 (Tac1) and tachykinin receptor 1 (Tacr1), two genes that are expressed in spinal projection neurons (Choi et al., 2020; Huang et al., 2019) (Figure S5).

### ErbB4+, SST+, and CCK+ neurons for heat sensation

Next, we ablated ErbB4+ neurons in bilateral spinal cords by Cre- and DIO-dependent expressions of diphtheria toxin subunit A (dtA) (Wu et al., 2014). ErbB4::CreER;LSL-EYFP (referred to as ErbB4-EYFP) mice were injected (intraspinal, i.s.) with AAV-mCherry-DIO-dtA (AAV-dtA for short) (Figure 2A). After tamoxifen activation of the Cre, dtA was expressed specifically in ErbB4+ cells (visualized by EYFP) (Figures 2B and 2D). As shown in Figure 2C, mCherry was detected in the dorsal horn of the lumbar region three weeks after viral injection. EYFP+ cells and Nmur2+ neurons were dramatically reduced in ErbB4-EYFP mice injected with AAV-dtA compared with mice injected with AAV-Ctrl (Figures 2D and 2E). This effect was specific because AAV-dtA infection had little effect on the numbers of INs that were positive for Pax2 and calretinin (CR) (Figure 2E). Next, mice were subjected to a battery of behavioral tests. The latencies of hind paw flinching and licking in hot plate test and paw withdrawal in Hargreaves test were increased by ~40% in AAV-dtA-injected ErbB4-EYFP mice compared with mice injected with AAV-Ctrl (Figures 2F and 2G), indicating that ErbB4+ neurons are critical to heat sensation. Capsaicin activates its receptor TRPV1 in sensory neurons to induce spontaneous pain (Caterina et al., 1997). Capsaicin-induced foot licking was reduced by 30% in AAV-dtA-injected ErbB4-EYFP mice compared with control (Figure 2H). These results reveal a requirement of ErbB4+ neurons for behavioral response to noxious heat. However, behavioral responses to mechanical stimulation by pinprick, pinch, and von Frey filaments and to stimuli such as cold, cool, warm, and itch (by histamine and chloroquine) were similar between AAV-dtA- and AAV-Ctrl-injected ErbB4-EYFP mice (Figure S6), suggesting that ErbB4+ neurons may not be involved in processing these modalities.

In addition to ErbB4+ neurons, SST+ and CCK+ INs were activated by noxious heat stimulation (Figures 1G, 1I, and 1K). To determine their contribution to heat sensation, we ablated these neurons individually and in combination with ErbB4+ neurons by injecting AAV-dtA into SST-Cre mice, CCK-Cre mice, or mice with three Cre (triple Cre, tri-Cre) (Figures 2I and 2J). As shown in Figures 2K and 2L, the response latency in hot plate and Hargreaves tests was increased (26% or 22%, respectively) by the ablation of SST+ neurons, but not of CCK+ neurons. However, the ablation of SST+ or CCK+ neurons had little effect on capsaicin-induced foot licking (Figure 2M). Remarkably, the inhibitory effect was dramatically increased to 60%–80% when the three populations of neurons were ablated simultaneously compared with AAV-mCherry-injected tri-Cre mice (Figures 2I–2M). The ablation of individual populations or in combination had little effect on behaviors in the rotarod test or cold-induced foot withdrawal reflex (Figures 2N and 2O). These results suggest that heat sensation involves ErbB4+, SST+, and CCK+ neurons in the spinal cord, in support of the population model.

### Monosynaptic innervation by TRPV1+ nociceptors

Different somatosensory information is transmitted by different types of afferent fibers into the dorsal horn: A $\beta$  fibers for innocuous, whereas A $\delta$  and C fibers for nociceptive signals (Julius and Basbaum, 2001). To characterize the inputs to ErbB4+ neurons, we recorded excitatory postsynaptic currents (EPSCs) in longitudinal spinal slices with attached dorsal roots of ErbB4::CreER;Ai9 mice (Figure S7A) (Duan et al., 2014; Pan et al., 2019). EPSCs were recorded in 76% and 54% of layer I/II ErbB4+ neurons in response to stimuli for A $\delta$  and C fibers, respectively (Figures S7B and S7C). In total, 67% and 46% of ErbB4+ neurons responded monosynaptically, respectively. In contrast, 25% of ErbB4+ neurons in layers I/II generated EPSCs to A $\beta$  fiber stimulation, and only 9.1% were monosynaptic. Moreover, A $\delta$  and C fiber stimulation elicited monosynaptic responses in only 6.7% and 5.6% of deep-layer ErbB4+ neurons, respectively (Figure S7C). These results indicate that ErbB4+ neurons in superficial layers mainly receive monosynaptic inputs from nociceptor-containing C and A $\delta$  fibers.

To test whether ErbB4+ neurons are synapsed by TRPV1+ neurons, we studied the effect of QX-314, an intracellular inhibitor of sodium channels whose cell entry depends on TRPV1 activation (Brenneis et al., 2013). As shown in Figures S7D and S7E, QX-314 alone had little effect on EPSC amplitudes of ErbB4+ neurons in response to C fiber stimulation (compared with vehicle, Veh). However, the EPSCs were diminished by QX-314 in the presence of the TRPV1 activator capsaicin (Figures S7D and S7E), suggesting that ErbB4+ neurons are innervated by TRPV1+ fibers. In agreement, the number of ErbB4+ neurons responsive to C fiber stimulation was reduced (from 57% to 9.1%) in the presence of QX-314 and capsaicin (Figure S7E). This effect was C-fiber specific as QX-314 showed little effect on EPSCs by stimulating A $\beta$  and A $\delta$  fibers whose expression of

(J) shEGFP+ cells positive of ErbB4.

(K) Vglut2+ shEGFP+ cells that were positive of ErbB4 and other IN markers.

(L–N) Activation of ErbB4+ neurons in superficial dorsal horn by noxious heat. (M) cFos expression in tdTomato-labeled ErbB4+ cells in area indicated in (L). Scale bar, 30  $\mu$ m. (N) Increased tdTomato+ cFos+ cells by exposure to 52°C hot plate; t test, \*\*\*p < 0.001; n = 12 slices of 3 mice.

(O) tdTomato+ cFos+ cells in deep layers. t test, n = 12 slices of 3 mice.

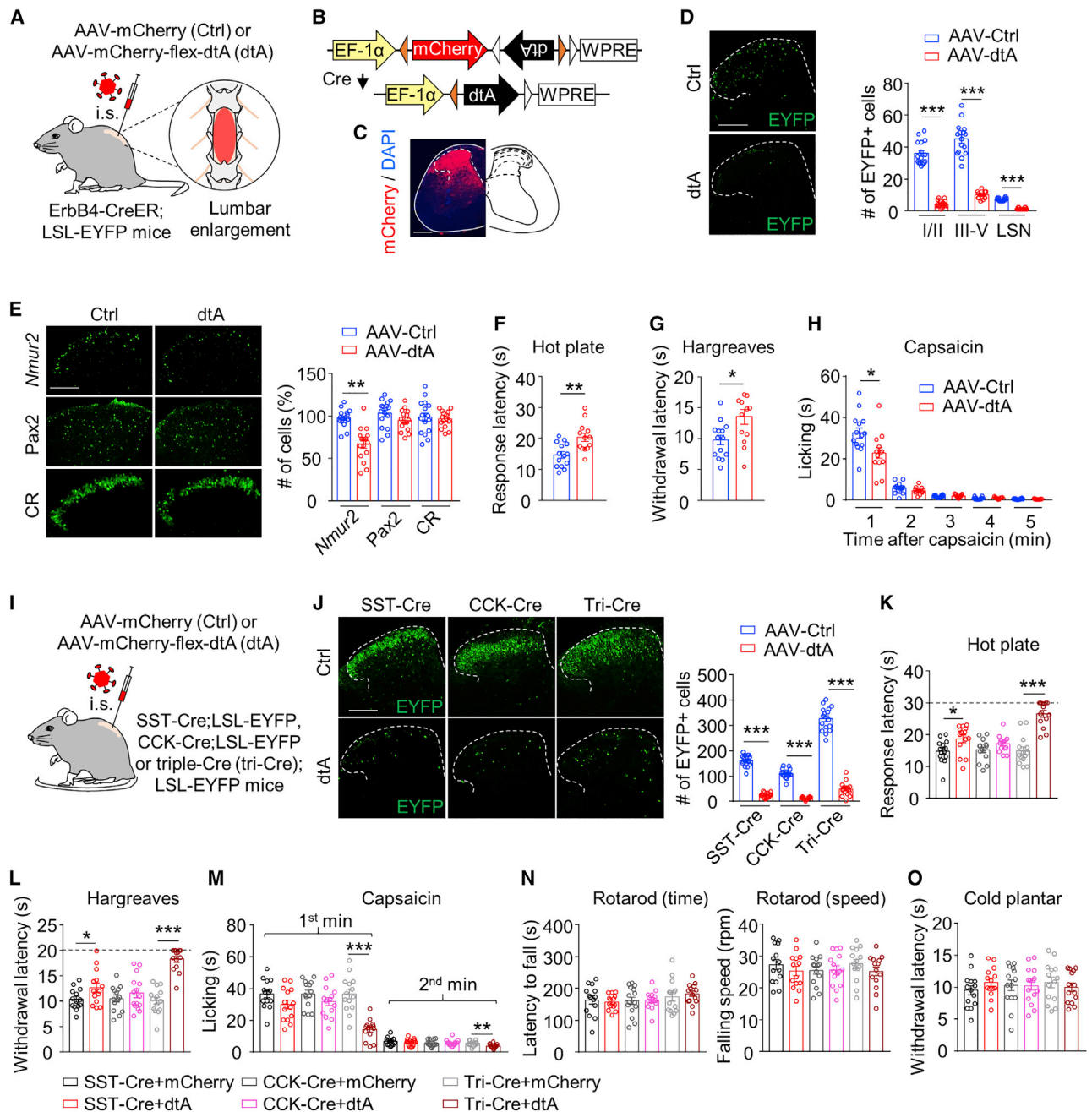


**Figure 2. Diminished heat sensation by ablating ErbB4<sup>+</sup> neurons**

(A) Diagram of viral injection and genotype of mice. i.s., intraspinal injection.  
 (B) Diagrams of Cre-dependent expression by AAV.  
 (C) Validation of AAV-mCherry expression in dorsal horn areas of lumbar enlargements. Scale bar, 300  $\mu$ m.  
 (D) Ablation of EYFP<sup>+</sup> cells in lumbar enlargements 3 weeks after AAV-dtA injection. Left, example images; right, quantification result. t test, \*\*\*p < 0.001; n = 16 slices of 4 mice. Scale bar, 250  $\mu$ m.  
 (E) Reduced *Nmur2*<sup>+</sup> cells and no change in *Pax2*<sup>+</sup> and *CR*<sup>+</sup> cells by AAV-dtA. Left, example images of RNAscope of *Nmur2* and immunostaining of *Pax2* and *CR*. Scale bar, 200  $\mu$ m; right, quantitative data. t test, \*\*p = 0.0017; n = 16 slices of 4 mice. Scale bar, 250  $\mu$ m.  
 (F–H) AAV-dtA-injected ErbB4-CreER; LSL-EYFP mice showed increased latency in hot plate test (F, t test, \*\*p = 0.002); increased latency in Hargreaves test (G, t test, \*p = 0.024) and reduced capsaicin-induced foot licking (H, t test, \*p = 0.0136).  
 (I) Diagram of viral injection and genotype of mice.

(legend continued on next page)

TRPV1 is low (Cavanaugh et al., 2011) (Figures S7D and S7E). These results provide pharmacological evidence that ErbB4+ neurons in the superficial layers are innervated by TRPV1+ C fibers. To provide morphological evidence for this innervation, TRPV1::Cre;ErbB4::CreER mice were injected with AAV-DIO-mCherry into the lumbar enlargement to label ErbB4+ neurons and with AAV-DIO-ChR2-EYFP into the DRGs to label TRPV1+ terminals (Figure 3A). Spinal cord sections were stained with antibodies against Homer, a postsynaptic marker (Gutierrez-Mecinas et al., 2016). As shown in Figure 3B, ErbB4+ (i.e., mCherry+) neurons were surrounded by EYFP+ (i.e., TRPV1+) terminals. The intraspinal AAV injection is likely to have retrograde infection (Haenraets et al., 2017) and may thus label DRG neurons. However, mCherry fluorescence or protein was not detectable in the DRG (data not shown). Nevertheless, TRPV1+ terminals were in close registry with both Homer+ puncta and ErbB4+ cells (Figure 3B). These results further suggest that ErbB4+ neurons were synapsed by TRPV1+ DRG neurons.

To demonstrate that these synapses are functional, we activated ErbB4+ neurons by optogenetic stimulation. Capsaicin-responsive DRG neurons in culture of virus-injected mice produced photocurrents and action potentials (APs) by optical stimulation (473 nm) (Figures S8A–S8F). Optical stimulation of longitudinal spinal cord slices evoked EPSCs in 42% layer I/II ErbB4+ neurons, which were inhibited by TTX, suggesting a requirement of APs (Figures 3D–3F). To determine monosynaptic innervation, slices were incubated with TTX and 4-AP, a potassium channel blocker that facilitates depolarization of nerve terminals (Petreanu et al., 2009; Rodriguez et al., 2017). As shown in Figures 3D–3F, 36% of ErbB4+ layer I/II neurons exhibited evoked EPSCs in the presence of both TTX and 4-AP, demonstrating that they are innervated monosynaptically by TRPV1+ DRG neurons. As a control, only 3.7% of ErbB4+ neurons in deep layers displayed monosynaptic EPSCs from TRPV1+ DRG neurons (Figures 3D and 3E). Together, these morphological and functional results indicate that ErbB4+ neurons in superficial layers are innervated directly by TRPV1+ nociceptors.

### Activation by heat but not mechanical stimulation

To determine whether ErbB4+ neurons respond to the activation of mechanosensory DRG neurons, we used MrgprD::CreER mice, where Cre is driven by the promoter of MrgprD that is expressed in DRG neurons critical for mechanosensitivity (Figure 3G) (Olson et al., 2017). MrgprD::CreER;ErbB4::CreER mice were injected with AAV-DIO-ChR2-EYFP into the DRGs to express ChR2 in DRG neurons and with AAV-DIO-mCherry into the lumbar enlargement to label ErbB4+ neurons (Figure 3G). Optical stimulation of cultured EYFP+ DRG neurons from injected mice produced photocurrents and APs (Figures S8G–S8J), indicative of ChR2 expression in MrgprD+ neurons. However, optical stimulation of spinal cord slices failed to evoke

EPSCs in 19 of 22 (87%) recorded lamina I/II ErbB4+ neurons, indicating that a majority of ErbB4+ neurons do not receive inputs from mechanosensory neurons (Figures 3H, 3J, and 3K). Among the 3 responsive ErbB4+ neurons, 2 (9%) were inhibited by TTX and 4-AP, suggesting that they receive polysynaptic inputs (Figures 3H, 3J, and 3K). Only one of 22 (5%) ErbB4+ neurons produced EPSCs that were potentiated by 4-AP, indicative of monosynaptic input (Figures 3H, 3J, and 3K). As a control, we used the same strategy to characterize the responses of SST+ spinal neurons to mechanosensory neuron stimulation (Figures 3G and 3I). Most of recorded SST+ neurons (72%, 13/18) produced light-evoked EPSCs, suggesting that they are innervated by MrgprD+ DRG neurons, 61% (11/18) of which were monosynaptic (Figures 3J and 3K), in agreement with previous reports (Duan et al., 2014). Together with the studies of TRPV1 inputs (Figures 3A–3F), these results suggest that layer I/II ErbB4+ neurons are mostly innervated by heat nociceptive DRG neurons, not by mechanosensory neurons.

To further characterize the sensitivity of ErbB4+ neurons in a more physiological condition, we established a semi-intact *ex vivo* preparation consisting of a portion of spinal cord together with lumbar roots, DRGs, saphenous nerve, and hindlimb skin (Figure 3L) (Choi et al., 2020; Hachisuka et al., 2016). This preparation enables the analysis of modality specificity by recording spinal neurons in response to natural stimulation of sensors in the skin (Choi et al., 2020; Hachisuka et al., 2016). We recorded APs in layer I/II ErbB4+ neurons in the semi-intact preparation from ErbB4::CreER;Ai9 mice (Figure 3L). Of the 16 neurons recorded, 9 (56%) responded to 52°C stimuli, and 5 (30%) responded to 0°C stimuli (Figures 3M–3P). The number of responsive neurons to 15°C and 40°C were 1 (7%) and 2 (13%), respectively (Figures 3M–3P). These results indicate that lamina I/II ErbB4+ neurons respond preferably to noxious heat, followed by cold stimuli, and they are less responsive to cool or warm stimuli. To determine whether ErbB4+ neurons respond to mechanical stimulation, the skin was stimulated with von Frey filaments (1.0–4.0 g). As shown in Figures 3M–3P, mechanical stimulation failed to produce APs in 14 of 16 recorded neurons. As controls, 7 (58%) of 12 SST+ neurons (from SST-Cre;Ai9 mice) responded with APs by mechanical stimulation (Figure S9), in agreement with previous reports (Duan et al., 2014). Notice that 3 (25%) of 12 SST+ neurons responded to noxious heat stimulation (Figures 3M–3P), in support of the population-coding hypothesis. Together, these observations demonstrate that ErbB4+ neurons in superficial layers are more responsive to noxious heat than mechanical stimulation.

### ErbB4+ neuron inhibition reduces heat response, while activation increases heat response

Next, we studied the impact of altering the activity of ErbB4+ neurons by designer receptor electively activated by designer

(J) Ablation of EYFP+ cells in lumbar enlargements 3 weeks after AAV-dtA injection. Left, example images; right, quantification data. Scale bar, 250  $\mu$ m. t test, \*\*\*p < 0.001. n = 16 slices of 4 mice.

(K–M) Alteration of indicated mice in latency in hot plate test (K) (dashed line, the cutoff time; t test, \* $p_{(SST)} = 0.0184$ , \*\*\* $p_{(tri)} < 0.001$ ); latency in Hargreaves test (L) (dashed line indicates the cutoff time; t test, \* $p_{(SST)} = 0.039$ , \*\*\* $p_{(tri)} < 0.001$ ); and capsaicin-induced foot licking (M) (t test, \*\*\* $p_{(tri, 1st\ min)} < 0.001$ , \*\* $p_{(tri, 2nd\ min)} = 0.0029$ ).

(N and O) AAV-dtA had little effect on falling time (left) or speed (right) in rotarod test (N) and latency of foot withdrawal induced by cold (O). t test.

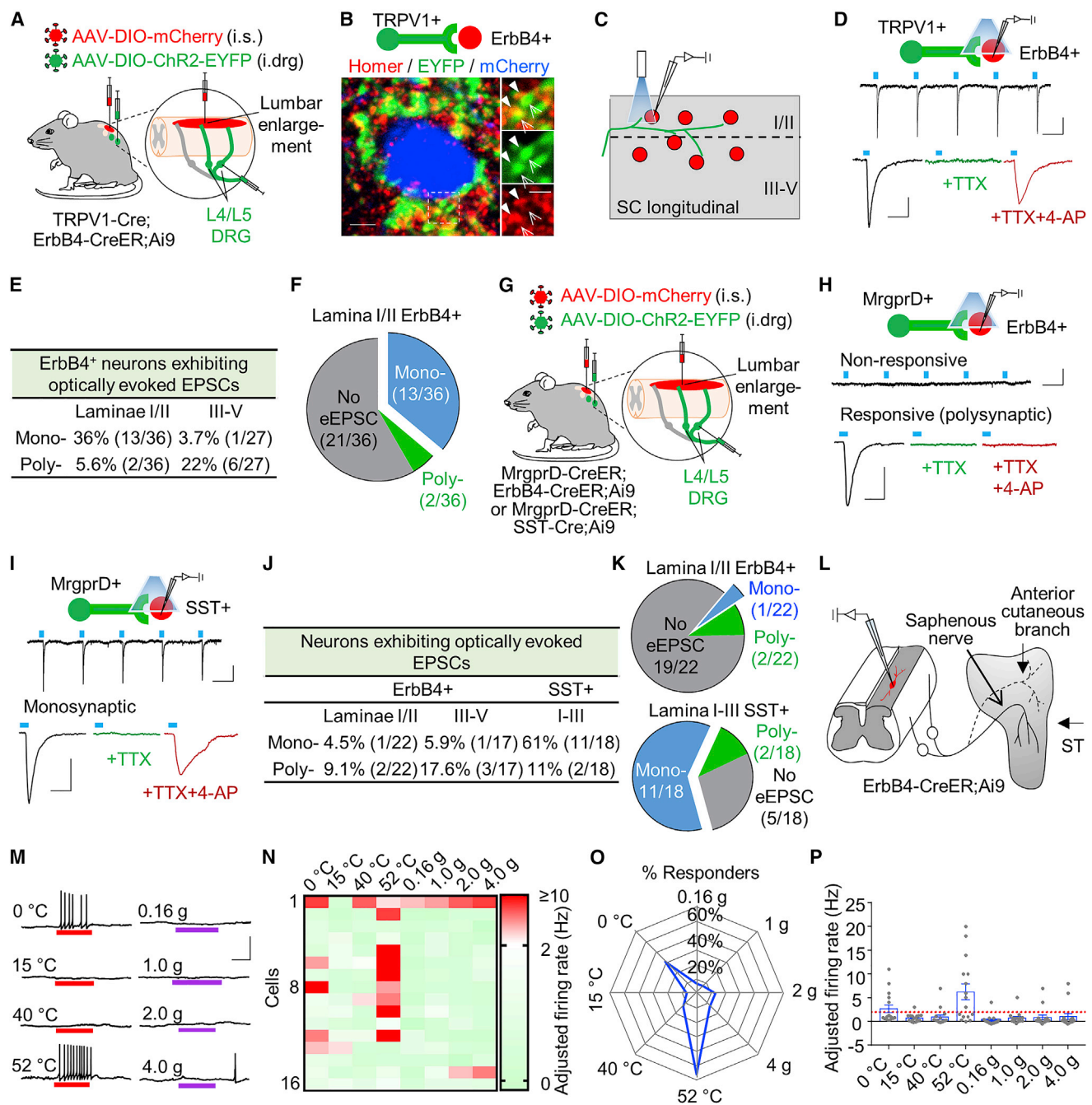


**Figure 3. Activation of ErbB4+ neurons by noxious heat but not mechanical stimulation**

(A–F) Monosynaptic inputs from TRPV1+ fibers onto ErbB4+ neurons. (A) Diagram of viral injection and genotype of mice. i.s., intraspinal, i.drg, intra-DRG injection. (B) EYFP+ terminals in close proximity to Homer+ puncta and mCherry+ (i.e., ErbB4+) cells in spinal slices. Scale bars, left, 2  $\mu$ m, right, 1  $\mu$ m. (C) Diagram of recording of ErbB4+ neurons in spinal slices. SC, spinal cord. (D) Example traces of light-evoked monosynaptic EPSCs in ErbB4+ neurons without (top) or with TTX and/or 4-AP (bottom). Scale bars, upper: 0.5 s, 50 pA; lower: 50 ms, 50 pA. (E and F) ErbB4+ neurons with monosynaptic or polysynaptic inputs from TRPV1+ DRG neurons. (G–K) Innervation of MrgprD+ neurons onto ErbB4+ neurons. (G) Diagram of viral injection and genotype of mice. (H) Example nonresponsive traces of ErbB4+ neurons (top: scale bars, 0.5 s, 50 pA) and light-evoked EPSCs without or with TTX and/or 4-AP (bottom: scale bars 50 ms, 100 pA). (I) Example traces of light-evoked monosynaptic EPSCs in SST+ neurons. EPSC resistance to TTX and 4-AP was shown in lower panel. Scale bars, upper: 0.5 s, 50 pA; lower: 50 ms, 100 pA. (J and K) ErbB4+ and SST+ neurons receiving monosynaptic or polysynaptic inputs from MrgprD+ DRG neurons. (L–P) Activation of ErbB4+ neurons by heat stimulation of skin. (L) Diagram showing recording of ErbB4+ cells in the semi-intact preparation with stimuli being applied to the skin. ST, stimulation. (M) AP traces in ErbB4+ neurons evoked by saline at different temperatures and von Frey filaments. Scale bars, 0.5 s, 50 mV. (N) Heatmap of ErbB4+ neuron responses. (O) Radar plot of responsive ErbB4+ neurons to each modality. (P) Firing rates in response to stimuli. Dashed line, threshold of 2 Hz.

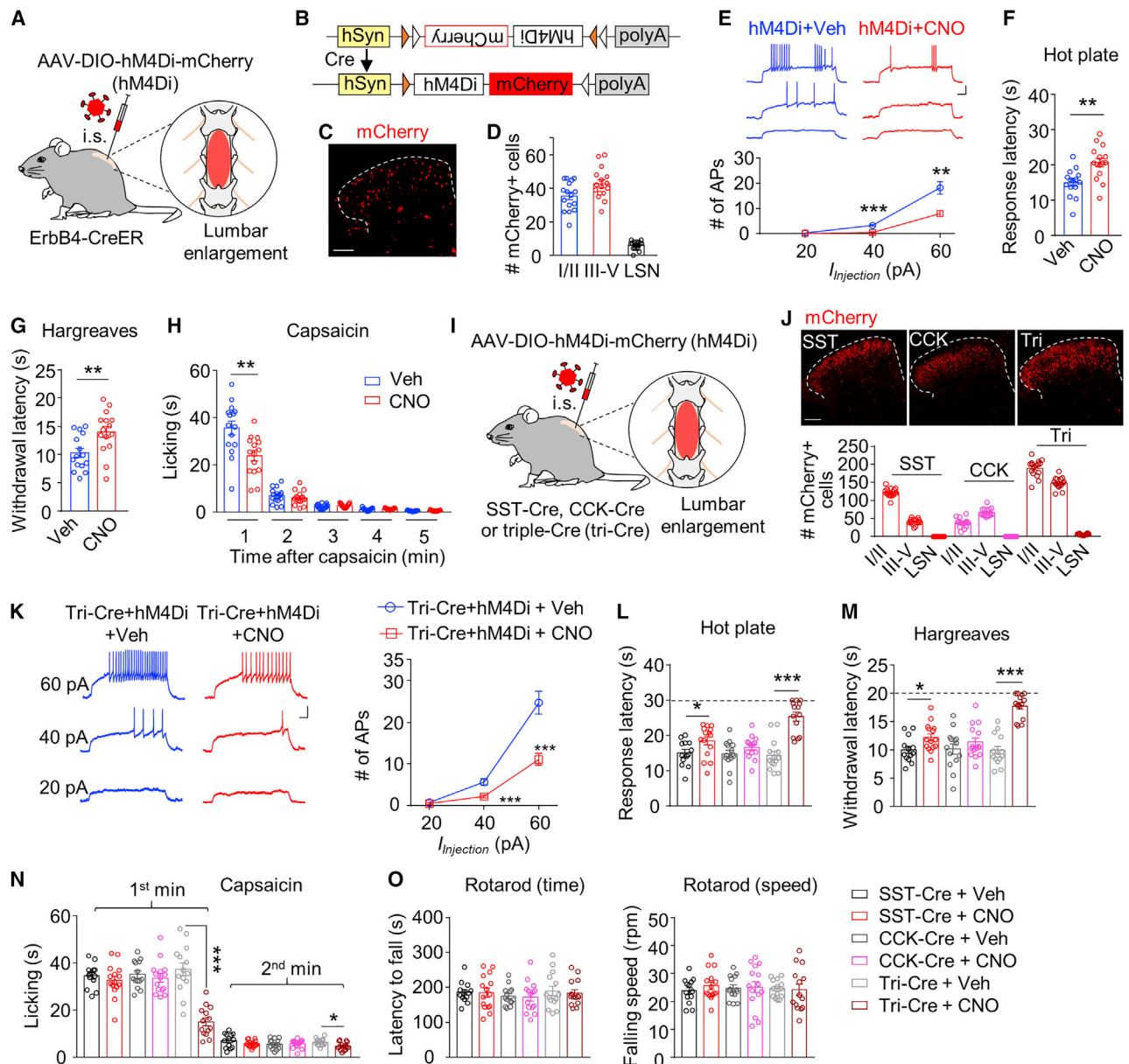


**Figure 4. Inhibition of ErbB4<sup>+</sup> neuron reduces heat response**

(A) Diagram of viral injection and genotype of mice. i.s., intraspinal injection.  
 (B) Diagram of Cre-dependent expression of AAV-hM4Di and mCherry.  
 (C) MCherry expression in injected lumbar enlargements. Scale bar, 100  $\mu$ m. n = 16 slices of 4 mice.  
 (D) mCherry<sup>+</sup> cells in the dorsal horn and LSN.  
 (E) CNO reduced APs in response to current injection in mCherry<sup>+</sup> (i.e., ErbB4<sup>+</sup>) neurons. Top: representative traces, scale bars, 100 ms, 20 mV; bottom: quantitative data. Slices were incubated with 1  $\mu$ M CNO for 10 min prior to recording. t test, \*\*\* $p_{(40 \text{ pA})} < 0.001$ , \*\* $p_{(60 \text{ pA})} = 0.0024$ . n = 10 cells of 3 mice.  
 (F and G) Increased response latency in hot plate (F) and Hargreaves (G) tests by CNO. AAV-hM4Di-injected ErbB4-CreER mice were treated with CNO (i.p., 5 mg/kg) 30 min prior to test. t test, \*\* $p_{(\text{hot plate})} = 0.0013$ , \*\* $p_{(\text{Hargreaves})} = 0.0074$ .  
 (H) Decreased capsaicin-induced foot licking by CNO. t test, \*\* $p = 0.0031$ .  
 (I) Diagram of AAV injection into lumbar enlargement of SST-Cre, CCK-Cre, or ErbB4-CreER; SST-Cre; CCK-Cre (tri-Cre) mice.  
 (J) mCherry expression in injected lumbar enlargements. Top: representative images; bottom: quantitative data. Scale bar, 100  $\mu$ m. n = 16 slices of 4 mice.  
 (K) CNO reduced APs in response to current injection in mCherry<sup>+</sup> neurons. Left, representative traces, scale bars, 100 ms, 20 mV; right, quantitative data. Slices were incubated with 1  $\mu$ M CNO for 10 min prior to recording. t test, \*\*\* $p_{(40 \text{ pA})} = 0.0006$ , \*\*\* $p_{(60 \text{ pA})} = 0.0003$ . n = 11 cells of 3 mice.

(legend continued on next page)

drugs (DREADD)-based chemogenetics (Figures 4 and S12). To reduce their activity, ErbB4::CreER mice were injected with AAV-DIO-hM4Di-mCherry (AAV-hM4Di) that directs Cre-dependent expression of hM4Di (Figure 4A) (Krashes et al., 2011), a modified G-protein coupled receptor, which upon activation by clozapine-N-oxide (CNO), increases the inward rectifier potassium currents and attenuates neuronal activity (Armbruster et al., 2007). After tamoxifen activation of the Cre, hM4Di and mCherry were expressed in ErbB4+ cells (Figures 4B–4D); CNO inhibited current injection-induced APs in ErbB4+ neurons in spinal cord slices of mice injected with AAV-hM4Di (Figure 4E), in a manner dependent on AAV injection (Figures S10A and S10B). CNO increased response latency in hot plate (39%) and Hargreaves tests (36%) and reduced capsaicin-induced foot licking (33%) in AAV-hM4Di-injected mice compared with Veh-treated mice (Figures 4F–4H). The effect of CNO was not observed in ErbB4::CreER;Ai9 mice without AAV injection (Figures S10C–S10E). Moreover, CNO had little effect on responses in tests for the mechanical, cold, cool, warm, or itch modalities (Figures S11A–S11H). These results suggest that the activity of ErbB4+ neurons is required for behavioral response to noxious heat. Inhibiting SST+ neurons, but not CCK+ neurons, increased the response latency in hot plate and Hargreaves tests (by 23% and 21%, respectively) but had little effect on capsaicin-induced foot licking (Figures 4I–4N). Notably, when the neuronal activity of all three populations was reduced, the inhibitory effect on the three tests was increased to 60%–80% compared with Veh-treated tri-Cre mice (Figures 4I–4N). Inhibition of individual populations or in combination had little effect on behaviors in the rotarod test (Figure 4O). Together with results from ablation studies (Figure 2), these results suggest that the activity of spinal ErbB4+, SST+, and CCK+ neurons jointly contributes to heat sensation, in support of the pattern theory.

To increase the activity of spinal ErbB4+ neurons, we expressed hM3Dq, a modified human M3 muscarinic receptor that upon activation by CNO, activates cells by increasing intracellular calcium (Armbruster et al., 2007). ErbB4::CreER mice were injected with AAV-DIO-hM3Dq-mCherry that directs Cre-dependent expression of hM3Dq and mCherry (Figures S12A–S12D) (Krashes et al., 2011). As shown in Figure S12E, CNO increased the firing of ErbB4+ neurons in spinal slices of AAV-hM3Dq-injected mice compared with Veh, demonstrating the feasibility of the DREADD strategy. CNO injection reduced the response latency in hot plate (31%) and Hargreaves tests (33%) in AAV-hM3Dq-injected ErbB4::CreER mice compared with Veh (Figures S12F and S12G). Consistently, the duration of capsaicin-induced foot licking was increased (29%) in the CNO-treated AAV-hM3Dq group (Figure S12H). These results indicate that increased activity of spinal ErbB4+ neurons could enhance heat sensation. This effect appeared to be selective because CNO had little effect on responses to mechanical, cold, cool, warm, or itch stimulation (Figures S11I–S11P).

Together, these observations reveal a critical role of ErbB4+ neuronal activity in heat sensation.

### ErbB4 and its dynamic activity for heat sensation

To test whether the NRG1-ErbB4 signaling is involved in heat sensation, we analyzed NRG1 and pErbB4 (phosphorylated ErbB4) in dorsal horns of the lumbar enlargement by ELISA and western blotting (Figure S13). Both were increased in 52°C plate-exposed mice compared with that of the 25°C group, suggesting that noxious heat stimulation at skin could enhance the NRG1-ErbB4 signaling in the spinal dorsal horn. Next, to determine whether ErbB4 is necessary, we crossed Stop-ErbB4 mice (Wang et al., 2018b) where ErbB4 transcription is blocked by a *loxP*-flanked stop signal between exons 1 and 2 with  $\alpha$ MHC::ErbB4 mice that express ErbB4 in the heart (to avoid lethality due to ErbB4's role in the heart) (Figure S14A). The resulting compound mice, ErbB4-rKO, do not express ErbB4 in any tissues, including the spinal cord except the heart (Figure S14B) (Wang et al., 2018b). Remarkably, ErbB4-rKO mice showed increased response latency in hot plate and Hargreaves tests and reduced foot licking induced by capsaicin compared with control ( $\alpha$ MHC::ErbB4) mice (Figures S14C–S14E), suggesting a role of ErbB4 in these responses. Responses in pinprick, pinch, and von Frey tests were similar between ErbB4-rKO and control mice (Figures S15A–S15D), suggesting that ErbB4 is dispensable for response to mechanical stimuli. Next, to eliminate a possible contribution of ErbB4 mutation in the other tissues, we deleted ErbB4 specifically in the spinal cord by injecting AAV-Cre-GFP (referred to as AAV-Cre) or AAV-GFP (as control) into the dorsal horn of the lumbar enlargement of ErbB4<sup>f/f</sup> mice (Figures 5A and 5B). Viral infection was verified by GFP expression (Figure 5C). ErbB4 was reduced in lumbar spinal cords of AAV-Cre-injected ErbB4<sup>f/f</sup> mice compared with control mice injected with AAV-GFP (Figure 5D). They showed increased latency in hot plate test and Hargreaves test and decreased foot licking induced by capsaicin compared with control mice (Figures 5E–5G). No difference was observed in pinprick, pinch, or von Frey test between the two groups (Figures S15E–S15H). These results reveal a necessary role of ErbB4 in the spinal cord in heat sensation.

To determine whether heat sensation involves the kinase activity of ErbB4, mice were injected (i.e., intrathecal, via puncture at vertebrae L5–L6) with afatinib, an inhibitor of ErbB kinases (Li et al., 2008). Afatinib reduced pErbB4 in the lumbar enlargement (Figures 5H and 5I). It also attenuated the response in hot plate, Hargreaves, and capsaicin tests (Figures 5J–5L), but it had little effect on the response to stimulation of pinprick, pinch, and von Frey filaments (Figures S15I–S15L). These results suggest the involvement of ErbB4 kinase activity in heat sensation. To further test this, we studied T796G mice, a knockin mutant strain where ErbB4 can be specifically inhibited by the bulky inhibitor 1NMPP1 (due to enlarged ATP binding pocket) (Figure 5M) (Robinson et al., 2022; Tan et al., 2018; Wang et al., 2021). T796G

(L and M) Increased response latency in hot plate and Hargreaves tests by CNO in AAV-hM4Di-injected SST-Cre and tri-Cre mice. Dashed lines indicate the cutoff time. t test. \* $p_{(SST, hot\ plate)} = 0.0373$ , \* $p_{(SST, Hargreaves)} = 0.0229$ ; \*\*\* $p_{(tri, hot\ plate)} < 0.001$ , \*\*\* $p_{(tri, Hargreaves)} < 0.001$ . (N) Decreased capsaicin-induced foot licking by CNO in tri-Cre mice. t test. \*\*\* $p_{(tri, 1st\ min)} < 0.001$ , \* $p_{(tri, 2nd\ min)} = 0.0109$ . (O) Little changes in falling time (left) or speed (right) in rotarod test. t test.

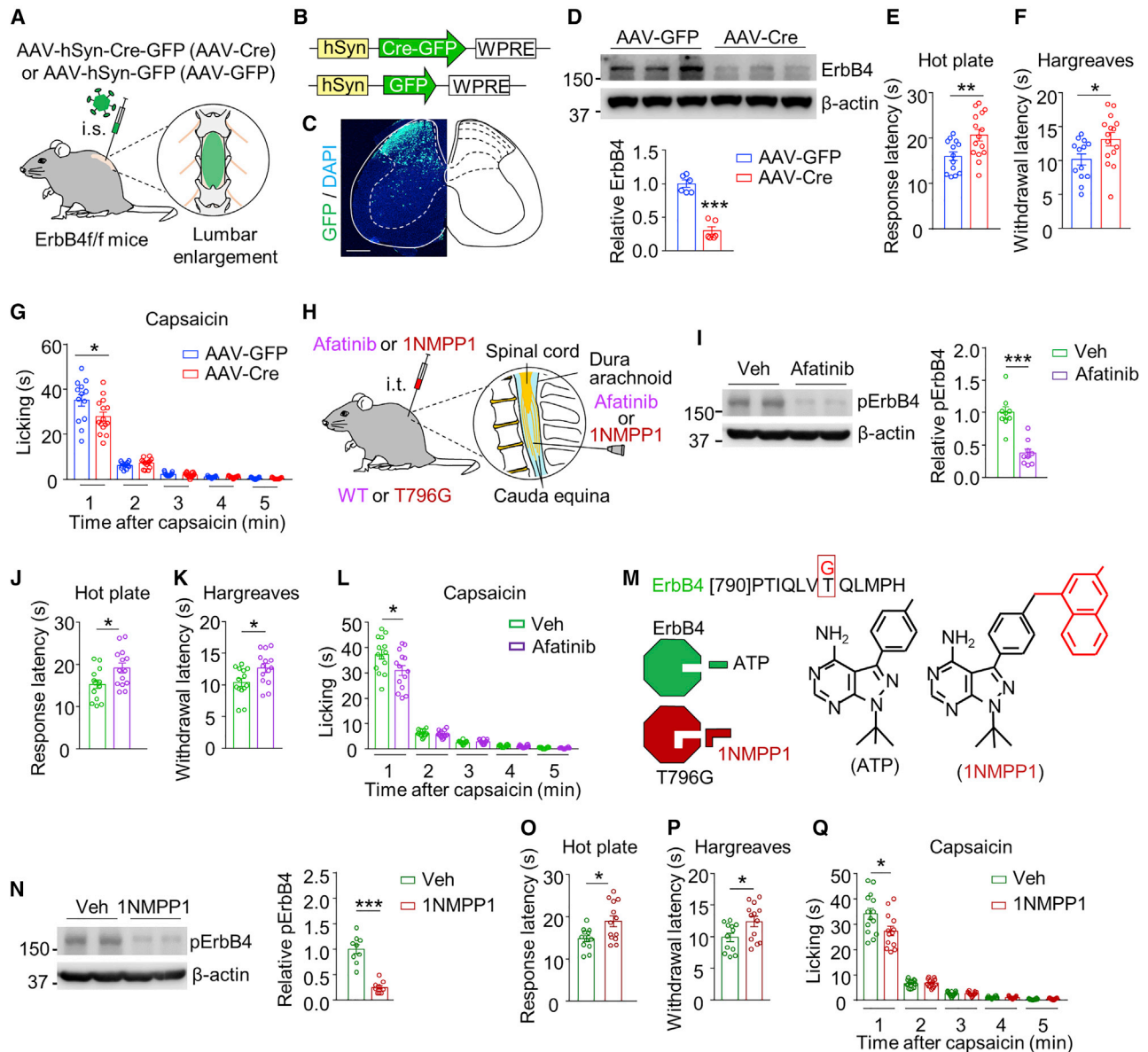


**Figure 5. Involvement of spinal ErbB4 and its kinase activity in heat sensation**

(A–G) Requirement of ErbB4. (A) Diagram of viral injection (i.s., intraspinal) and genotype of mice. (B) Diagram of AAV-Cre and AAV-GFP. (C) AAV expression in lumbar enlargements. Scale bar, 250  $\mu$ m. (D) Reduced ErbB4 expression in dorsal horns of lumbar enlargements. Tissues were dissected three weeks after viral injection. t test, \*\*\* $p$  < 0.001.

(E and F) Increased response latency in hot plate (E) and Hargreaves (F) test in AAV-Cre-injected ErbB4f/f mice. t test, \*\* $p$ (hot plate) = 0.0087, \* $p$ (Hargreaves) = 0.0284.

(G) Reduced capsaicin-induced foot licking in AAV-Cre-injected ErbB4f/f mice. t test, \* $p$  = 0.0351.

(H–L) Inhibition by afatinib. (H) Diagram of intrathecal injection. (I) Reduced pErbB4 by afatinib (2  $\mu$ M, 8  $\mu$ L) in lumbar enlargements of WT mice. Tissues were collected 30 min after injection. t test, \*\*\* $p$  < 0.001. Behavioral tests were performed 30 min after intrathecal injection. (J and K) Increased response latency in hot plate (J) and Hargreaves (K) tests in afatinib-injected WT mice; t test, \* $p$ (hot plate) = 0.0181; \* $p$ (Hargreaves) = 0.0206. (L) Reduced capsaicin-induced foot licking in afatinib-injected WT mice; t test, \* $p$  = 0.0286.

(M–Q) Inhibition by 1NMPP1. (M) Diagram of enlarged ATP binding pocket of ErbB4 T796G mutant. (N) Reduced pErbB4 in lumbar enlargements of T796G mice by 1NMPP1 (2  $\mu$ M, 8  $\mu$ L intrathecally injected 30 min prior to tissue dissection). t test, \*\*\* $p$  < 0.001. Behavioral tests were performed 30 min after intrathecal injection of 1NMPP1. (O) Increased latency of foot licking and flinching in hot plate test in 1NMPP1-injected T796G mice; t test, \* $p$  = 0.0119. (P) Increased latency of foot withdrawal in Hargreaves test in 1NMPP1-injected T796G mice; t test, \* $p$  = 0.0254 mice. (Q) Reduced capsaicin-induced foot licking in 1NMPP1-injected T796G mice; t test, \* $p$  = 0.025.

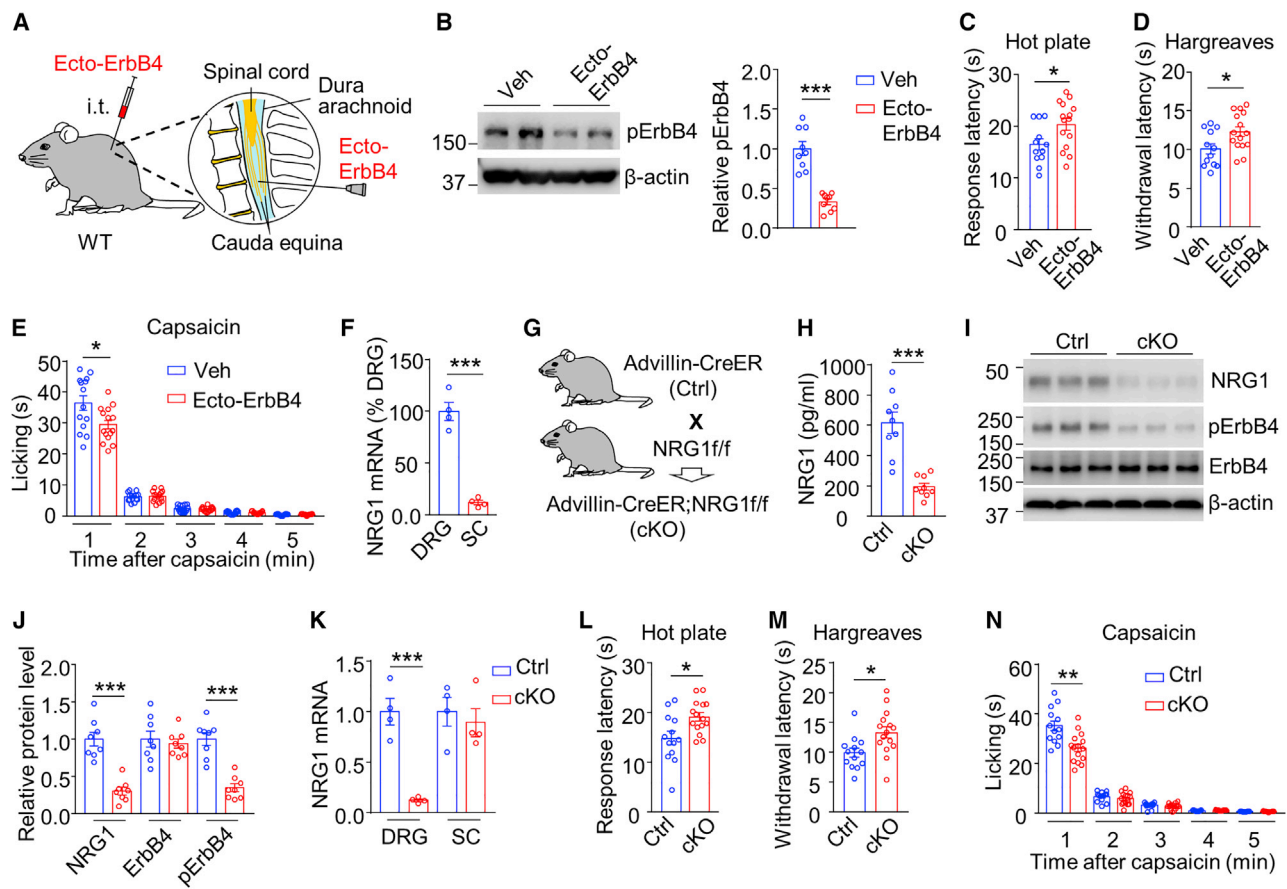


**Figure 6. Attenuated response to noxious heat by neutralizing endogenous NRG1 in spinal cord or deleting NRG1 in DRGs**

(A) Diagram of intrathecal injection.  
 (B) Reduced pErbB4 by ecto-ErbB4 in lumbar enlargements. Ecto-ErbB4 (5  $\mu$ g in 8  $\mu$ l) was intrathecally injected 1 h prior to tissue dissection. t test, \*\*\* $p$  < 0.001.  
 (C–E) Behavioral tests were performed 1 h after intrathecal injection. (C and D) Increased response latency in hot plate (C) and Hargreaves (D) tests in ecto-ErbB4-injected mice. t test, \* $p$ <sub>(hot plate)</sub> = 0.0258; \* $p$ <sub>(Hargreaves)</sub> = 0.0232. (E) Reduced capsaicin-induced foot licking in ecto-ErbB4-injected mice; t test, \* $p$  = 0.0146.  
 (F) More NRG1 mRNA in DRG than spinal dorsal horn. SC, spinal cord. t test, \*\*\* $p$  < 0.001. The content of NRG1 was calibrated with GAPDH.  
 (G) Breeding paradigm.  
 (H) ELISA showing reduced NRG1 protein in the spinal dorsal horn of advillin-CreER;NRG1f/f mice. t test, \*\*\* $p$  < 0.001.  
 (I and J) Reduced NRG1 protein and pErbB4 in the spinal dorsal horn of advillin-CreER;NRG1f/f mice. t test, \*\*\* $p$  < 0.001.  
 (K) Reduced NRG1 mRNA in DRG, but not spinal cord, of advillin-CreER;NRG1f/f mice. t test, \*\*\* $p$  < 0.001.  
 (L–N) Increased response latency in hot plate (L) and Hargreaves (M) tests and reduced duration of capsaicin-induced foot licking (N) in advillin-CreER;NRG1f/f mice. t test. \* $p$ <sub>(hot plate)</sub> = 0.011; \* $p$ <sub>(Hargreaves)</sub> = 0.0119; \*\* $p$ <sub>(capsaicin)</sub> = 0.0012.

mice showed no difference in responses to noxious heat or other sensation stimuli compared with wild-type control mice (data not shown). Intrathecal injection of 1NMPP1 reduced pErbB4 in the lumbar enlargement (Figure 5N). Because ErbB4 inhibition by 1NMPP1 is transient, behavioral tests were performed 30 min after injection when inhibition was maximal. 1NMPP1 displayed similar behavioral effects to afatinib (Figures 5O–5Q and S15M–S15P). Together, these results indicate that ErbB4 kinase activity in the spinal cord is involved in heat sensation.

### Involvement of DRG-derived NRG1

To determine whether heat sensation involves endogenous NRG1, mice were injected with ecto-ErbB4, a NRG1 neutralizing peptide (Krivosheya et al., 2008; Woo et al., 2007). Intrathecal injection of ecto-ErbB4 reduced pErbB4 in the spinal cord

(Figures 6A and 6B). It increased response latency in hot plate and Hargreaves tests and reduced foot licking due to capsaicin (Figures 6C–6E), but it had little effect on responses in pinprick, pinch, and von Frey tests (Figures S15Q–S15T). These results demonstrate that endogenous NRG1 is involved in noxious heat sensation, but not in mechanical sensation.

NRG1 is abundantly expressed in DRGs compared with dorsal horns (Calvo et al., 2010) (Figure 6F). To determine whether NRG1 from DRG neurons is involved in heat sensation, we crossed NRG1f/f mice with advillin-CreER mice (Figure 6G), where CreER is expressed in sensory ganglia (Hasegawa et al., 2007). The compound mice advillin-CreER;NRG1f/f were treated with tamoxifen (referred to as cKO). Compared with tamoxifen-treated NRG1f/f mice (control), NRG1 protein and pErbB4 were reduced in the spinal cord of cKO mice (Figures 6H–6J); NRG1 mRNA was reduced

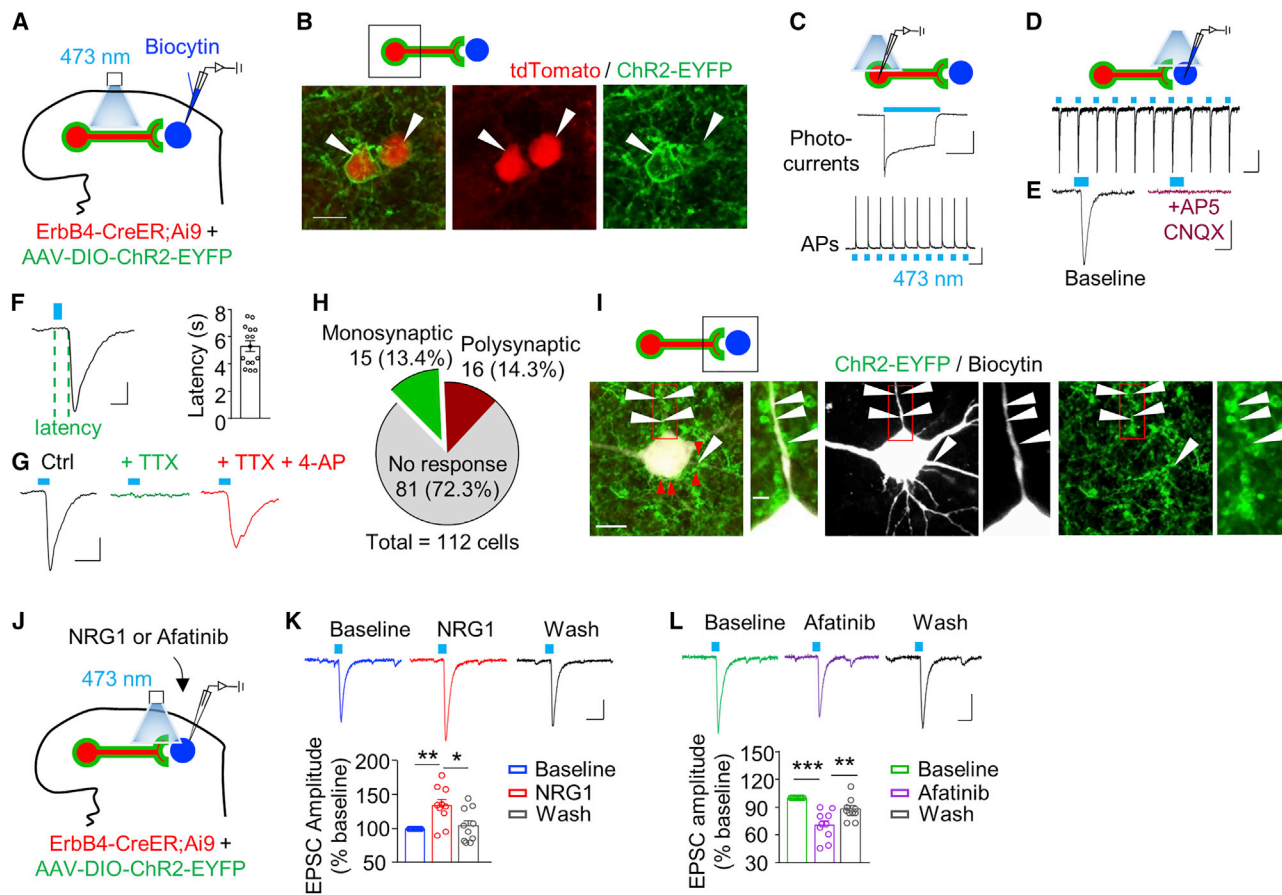


**Figure 7. NRG1-ErbB4 signaling promotes glutamatergic transmission**

(A–I) Glutamatergic transmission by ErbB4<sup>+</sup> neurons to downstream neurons in spinal cord slices. (A) Diagram of optogenetic activation of ErbB4<sup>+</sup> neurons and EPSC recording in downstream neurons. (B) Expressions of ChR2 and EYFP in ErbB4<sup>+</sup> neurons. Scale bar, 10  $\mu$ m. (C) Example traces of light-evoked photocurrents (upper) and APs (lower) in ErbB4<sup>+</sup> neurons under voltage-clamp and current-clamp modes, respectively. Scale bars, upper: 0.5 s, 100 pA; lower: 0.5 s, 20 mV. (D–H) Light-evoked glutamatergic EPSCs in neurons downstream. (D and E) Light (473 nm)-evoked EPSC traces without (top; bars, 0.2 s, 50 pA) and with glutamate antagonists (E), scale bars, 20 ms, 50 pA. (F) Short onset latency of EPSCs recorded in downstream neurons. Scale bars, 10 ms, 100 pA. (G) EPSCs resistant to TTX and 4-AP. Scale bars, 20 ms, 100 pA. (H) Quantitative data in (D)–(G).

(I) Innervation of biocytin-labeled neurons by ErbB4<sup>+</sup> neurons. Recorded neurons were labeled by biocytin in recording pipette and examined for EYFP<sup>+</sup> puncta (encoded by Cre-dependent AAV). Scale bars, 10 and 2  $\mu$ m for lower- and higher-power images, respectively.

(J) Diagram of recording.

(K) Increased amplitudes of light-evoked EPSCs in downstream neurons by NRG1 (10 nM). Upper: representative traces, scale bars, 20 ms, 40 pA; lower: quantitative data. Repeated measures one-way ANOVA, \*\* $p_{\text{baseline vs. NRG1}} = 0.0065$ , \* $p_{\text{wash vs. NRG1}} = 0.0186$ ; n = 10 cells of 3 mice.

(L) Afatinib (10 nM) reduced the amplitude of light-evoked EPSCs in downstream neurons. Upper: representative traces, scale bars, 20 ms, 40 pA; lower: quantitative data. Repeated measures one-way ANOVA, \*\*\* $p_{\text{baseline vs. afatinib}} < 0.001$ , \*\* $p_{\text{wash vs. afatinib}} = 0.0074$ ; n = 10 cells of 3 mice.

in DRG, but not in the spinal cord of cKO mice (Figure 6K). cKO mice exhibited increased response latency in hot plate and Hargreaves tests and reduced foot licking in capsaicin test (Figures 6L–6N). However, knockdown of NRG1 in the spinal cord had little effect on behavioral responses to heat stimuli, NRG1, or pErbB4 in dorsal horn (Figure S16). Together, these results suggest a role for DRG-generated NRG1 in noxious heat sensation.

### NRG1 and ErbB4 regulations of glutamatergic transmission in spinal cord

In the brain, NRG1 activates ErbB4 to promote GABA release from ErbB4<sup>+</sup> INs (Mei and Nave, 2014). Unexpectedly, the major-

ity of c-Fos<sup>+</sup> ErbB4<sup>+</sup> neurons in layer I/II are excitatory INs (Figure 1K). To determine whether NRG1 and ErbB4 regulate glutamatergic transmission, AAV-DIO-ChR2-EYFP was injected into ErbB4::CreER;Ai9 mice (Figure 7A) to express ChR2 in ErbB4<sup>+</sup> cells. Light stimulation produced photocurrents and APs in tdTomato<sup>+</sup> (i.e., ErbB4<sup>+</sup>) cells in transverse sections (Figures 7B and 7C) and postsynaptic currents in tdTomato<sup>-</sup> (i.e., ErbB4<sup>-</sup>) neurons in proximity to tdTomato<sup>+</sup> (i.e., ErbB4<sup>+</sup>) neurons (Figures 7A and 7D). Of 112 tdTomato<sup>-</sup> neurons, 31 generated inward currents when the membrane potential was clamped at -70 mV (Figures 7D and 7H). Light stimulation did not generate outward currents (clamp at 0 mV) in these neurons (data not shown), suggesting that the currents were EPSCs, not

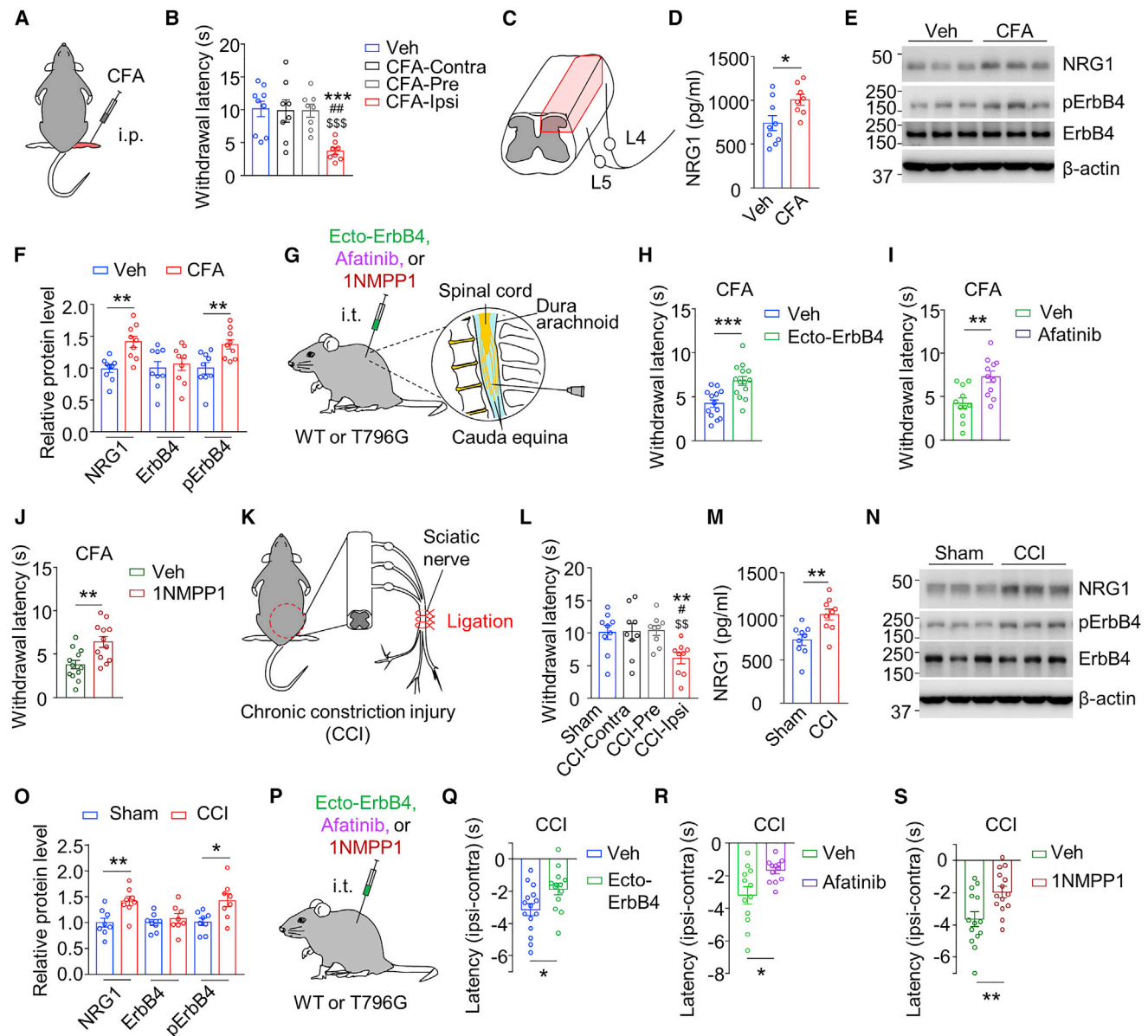


**Figure 8. Involvement of NRG1-ErbB4 signaling in heat hypersensitivity induced by peripheral inflammation and nerve injury**

(A) Diagram of a CFA model. i.p., intraplantar injection.

(B) Reduced withdrawal latency of CFA-injected hind paw in response to radiant heat in Hargreaves test. Veh, vehicle; ipsi, ipsilateral hind paw; contra, contralateral hind paw; pre, before CFA injection. t test,  $***p_{(\text{Veh vs CFA})} < 0.001$ ,  $^{##}p_{(\text{Contra vs Ipsi})} = 0.002$ ;  $^{$$$}p_{(\text{Pre vs Post})} < 0.001$ .

(C) Dissection of the spinal dorsal horn ipsilateral to the CFA injection.

(D) ELISA showing increased NRG1 protein in the ipsilateral dorsal horn of CFA mice. t test,  $*p = 0.025$ .

(E and F) Western blot showing increased NRG1 protein and pErbB4 in the ipsilateral dorsal horn. (E) Representative bands and (F) quantitative data. t test,  $**p_{(\text{NRG1})} = 0.0011$ ,  $**p_{(\text{pErbB4})} = 0.0064$ .

(G) Diagram of intrathecal injection.

(H–J) Increased withdrawal latency of the CFA-injected hind paw in mice injected with ecto-ErbB4 (H), afatinib (I), or 1NMPP1 (J). t test,  $***p_{(\text{ecto-ErbB4})} = 0.0008$ ;  $**p_{(\text{afatinib})} = 0.0028$ ;  $**p_{(\text{1NMPP1})} = 0.0038$ .

(K) Diagram of a CCI model.

(L) Reduced withdrawal latency of the CCI hind paw. Sham, sham surgery; ipsi, ipsilateral hind paw; contra, contralateral hind paw; and pre, before CCI surgery. t test,  $**p_{(\text{Sham vs CCI})} = 0.0097$ ;  $^{#}p_{(\text{Contra vs Ipsi})} = 0.0172$ ;  $^{$$}p_{(\text{Pre vs Post})} = 0.0016$ .

(M) ELISA showing increased NRG1 protein in the ipsilateral dorsal horn. t test,  $**p = 0.0043$ .

(N–O) Western blot showing increased NRG1 protein and pErbB4 in the ipsilateral dorsal horn. (N) Representative bands and (O) quantitative data. t test,  $**p_{(\text{NRG1})} = 0.0011$ ,  $**p_{(\text{pErbB4})} = 0.0064$ .

(P–Q) Diagram of intrathecal injection.

(R–S) Increased withdrawal latency of the CCI hind paw in mice injected with ecto-ErbB4 (R), afatinib (S), or 1NMPP1 (S). t test,  $**p_{(\text{ecto-ErbB4})} = 0.0008$ ;  $**p_{(\text{afatinib})} = 0.0028$ ;  $**p_{(\text{1NMPP1})} = 0.0038$ .

(legend continued on next page)

IPSCs. These results suggest that ErbB4+ neurons in superficial layers communicate with downstream neurons via glutamatergic transmission. Indeed, the EPSCs were blocked by CNQX (6-cyano-7-nitroquinoxaline-2,3-dione) and AP-5, inhibitors of AMPA ( $\alpha$ -amino-3-hydroxy-5-methyl-4-isoxazolepropionic acid) receptor and NMDA (N-methyl-D-aspartate) receptor, respectively (Figure 7E). Based on the onset latency and resistance to TTX and 4-AP (Figures 7F and 7G), half of downstream neurons received monosynaptic innervation from ErbB4+ neurons (Figure 7H). This notion is supported by morphological characterization of recorded neurons that were labeled with biocytin (Figure 7I). They were contacted by multiple EYFP+ puncta.

We next determined whether the glutamatergic transmission between ErbB4+ neurons and target cells is regulated by the NRG1-ErbB4 signaling (Figures 7J–7L). Remarkably, amplitudes of evoked EPSCs were increased by NRG1 (Holmes et al., 1992) within 15 min, and this effect was diminished after washout (Figures 7K and 7L), indicating that NRG1 promotes the glutamatergic transmission. Moreover, treatment of spinal slices with the ErbB4 inhibitor afatinib reduced EPSC amplitudes (Figures 7M and 7N), indicative of the involvement of ErbB4 kinase activity. Together, these data demonstrate a role for the NRG1-ErbB4 signaling in the glutamatergic transmission in the spinal cord.

### NRG1-ErbB4 signaling for heat hypersensitivity

Heat sensation is increased under pathological conditions such as peripheral inflammation and nerve injury. Injection of complete Freund's adjuvant (CFA), which causes inflammatory pain (Wang et al., 2020), reduced the withdrawal latency in Hargreaves test compared with contralateral or Veh-injected hind paws (Figures 8A and 8B). The following evidence suggest a role of NRG1-ErbB4 signaling in heat hypersensitivity induced by inflammation. First, NRG1 and pErbB4 were increased in ipsilateral lumbar enlargements in CFA-injected mice (Figures 8C–8F). Second, intrathecal neutralization of NRG1 (by ecto-ErbB4) increased foot withdrawal latency in Hargreaves test (Figures 8G and 8H). Third, heat hypersensitivity was inhibited by afatinib in wild-type mice (Figures 8G and 8I) and by 1NMPP1 in T796G mice (Figures 8G and 8J). We have also studied the potential involvement of this pathway in heat hypersensitivity induced by chronic constriction injury (CCI) (Taves et al., 2016) (Figure 8K). Compared with contralateral or sham-operated side, withdrawal latency in Hargreaves test was reduced in ipsilateral side of CCI mice (Figure 8L), indicating the development of heat hypersensitivity. NRG1 and pErbB4 were increased in ipsilateral lumbar enlargement of CCI group compared with sham-operated mice (Figures 8M–8O). To control potential individual variability to CCI, heat sensitivity of the ipsilateral side was normalized with that of the contralateral side. As shown in Figures 8P–8S, the heat hypersensitivity by CCI was attenuated by intrathecal injection of ecto-ErbB4 in wild-type mice (Figure 8Q), by afatinib in wild-type mice (Figure 8R), and by

1NMPP1 in T796G mice (Figure 8S) compared with Veh-injected mice. These results support the notion that the NRG1-ErbB4 signaling is involved in heat hypersensitivity induced by nerve injury. Finally, intrathecal injection of NRG1 to naive mice increased pErbB4 in lumbar segments and reduced response latency in Hargreaves tests compared with mice injected with Veh (Figures S17A–S17C), indicating that NRG1 is sufficient to increase heat sensitivity. This effect was attenuated by ErbB4 mutation or by 1NMPP1 in T796G mice (Figures S17D–S17G).

### DISCUSSION

By profiling noxious heat-responsive neurons, we identified the transmembrane tyrosine kinase ErbB4 as a marker of heat-sensitive spinal neurons in the superficial layers. These ErbB4+ neurons display the following properties. First, they mainly receive monosynaptic inputs from A $\delta$  and C fibers that are known to carry nociceptive signals, but not from A $\beta$  fibers that carry innocuous information (Julius and Basbaum, 2001). Second, ErbB4+ neurons are innervated monosynaptically by TRPV1+ neurons and respond preferably to noxious heat, but not to mechanical stimulation. Third, genetic ablation or chemogenetic inhibition of ErbB4+ neurons increases the latencies of hind paw flinching and licking in hot plate test and paw withdrawal in Hargreaves test and reduces capsaicin-induced foot licking, indicating that they and their activity are involved in heat sensation. Finally, we demonstrate a role for NRG1-ErbB4 signaling in heat sensation under physiological condition and hypersensitivity under pathological conditions.

Sensory information of individual modalities could be processed by specific neuronal circuits that transmit the signal from sensory organs to the brain (Cavanaugh et al., 2009; Emery et al., 2016; Hachisuka et al., 2020; Han et al., 2013; Knowlton et al., 2013; Norrsell et al., 1999). For example, mechanical pain, mechanical itch, and chemical itch are abolished by ablating or inhibiting spinal SST+, Ucn3+, and GRPR+ neurons, respectively (Duan et al., 2014; Pan et al., 2019; Sun et al., 2009), in support of the “labeled line” hypothesis. However, different IN populations are activated (with increased expression of phosphorylated ERK, cFos, or Arc) by noxious heat (Dickie et al., 2019; Gutierrez-Mecinas et al., 2019, 2017; Häring et al., 2018; Polgár et al., 2013). In agreement, besides ErbB4+ neurons that account for ~40% of cFos+ excitatory neurons, heat stimulation also activates SST+ and CCK+ neurons, which respectively represent 17% and 21% of cFos+ excitatory superficial-layer neurons. SST+ and CCK+ population each captures 22% of ErbB4+ cFos+ neurons, whereas ErbB4+ population captures 47% of SST+ cFos+ and 38% of CCK+ cFos+ cells. Behavioral responses to noxious heat stimulation were not abolished by ablating or inhibiting ErbB4+ neurons; however, the inhibitory effects are dramatically augmented by simultaneously ablating or inhibiting ErbB4+, SST+, and CCK+ neurons compared with

(N and O) Western blot showing increased NRG1 protein and pErbB4 in the ipsilateral dorsal horn. (N) representative bands and (O) quantitative data. t test, \*\* $p_{\text{NRG1}} = 0.0055$ , \* $p_{\text{pErbB4}} = 0.0123$ .

(P) Diagram showing intrathecal injection.

(Q–S) Increased withdrawal latency of the CCI hind paw in response to radiant heat stimulation in mice injected with ecto-ErbB4 (Q), afatinib (R), or 1NMPP1 (S). t test, \* $p_{\text{ecto-ErbB4}} = 0.0223$ , \* $p_{\text{afatinib}} = 0.0124$ , \*\* $p_{\text{1NMPP1}} = 0.0071$ .

manipulating only one group of neurons. The additive effects suggest that the three populations may act in parallel although further experiments are needed to determine whether SST+ and CCK+ cells receive direct inputs from TRPV1+ neurons or project to the brain. Nevertheless, a parsimonious interpretation of these results is that noxious heat is processed by joint activities of multiple types of neurons in the spinal cord, with ErbB4+ INs as a major substrate. These observations may favor the population-coding or pattern theory (Gatto et al., 2021; Häring et al., 2018; Paricio-Montesinos et al., 2020; Pogorzala et al., 2013). In agreement with our findings, behavioral responses to noxious heat were reduced, but not abolished, by the ablation of TRPV1+ DRG neurons in adult mice (Pogorzala et al., 2013).

NRG1 expression and maturation/release are dependent on neuronal activity (Eilam et al., 1998; Liu et al., 2011). It activates ErbB transmembrane kinases, including ErbB2, ErbB3, and ErbB4 (Mei and Nave, 2014; Mei and Xiong, 2008). In the cortex, hippocampus, and amygdala, ErbB4 is expressed in INs (Bean et al., 2014; Fazzari et al., 2010; Lin et al., 2018; Tan et al., 2018; Vullhorst et al., 2009; Woo et al., 2007) while a major source of NRG1 in adult brains is pyramidal neurons (Liu et al., 2011; Wang et al., 2021; Yao et al., 2021). The NRG1-ErbB4 pathway is critical to the assembly of GABAergic circuits, GABA transmission, and synaptic plasticity (Chen et al., 2010; Flames et al., 2004; Lu et al., 2014; Tan et al., 2011; Ting et al., 2011; Wen et al., 2010). In the peripheral nervous system, ErbB2 and ErbB3 are expressed in Schwann cells and activated by neuron-derived NRG1 for myelination (Meyer and Birchmeier, 1995; Michailov et al., 2004; Morris et al., 1999; Riethmacher et al., 1997; Taveggia et al., 2005). This study provides evidence that this signaling contributes to heat sensation. First, noxious heat stimulation rapidly increases NRG1 protein and ErbB4 activity (indicated by pErbB4) in the spinal lumbar enlargement. Second, responses to noxious heat are attenuated by global or lumbar enlargement-specific deletion of the ErbB4 gene and acute inhibition of the kinase (by afatinib and by 1NMPP1). On the other hand, intrathecal neutralization of endogenous NRG1 inhibits heat response, and injection of NRG1 enhances heat response. Together, these results suggest that the NRG1-ErbB4 pathway needs to be kept at an optimal level for heat sensation, identifying a novel physiological function of the NRG1-ErbB4 signaling. The source of NRG1 remains unclear, although deleting the NRG1 gene in DRG neurons attenuated heat sensation. NRG1 is mainly produced in myelinated neurons and less in TRPV1+ nociceptors (Calvo et al., 2010; Velanac et al., 2012; Willem et al., 2006). Future cell-type specific deletion of NRG1 will help to elucidate which cells produce NRG1 in response to heat stimulation. The mechanisms by which the NRG1-ErbB4 pathway promotes heat sensation remain unclear. Unlike ErbB4+ neurons in the cortex and hippocampus that are GABAergic, ErbB4+ neurons in spinal superficial layers are glutamatergic. Their transmission to downstream neurons requires NRG1-ErbB4 signaling. Moreover, whether NRG1 acts via non-neuronal components warrants future studies.

Somatosensory hypersensitivity is a common symptom in pathological pain conditions (Colloca et al., 2017; Merskey, 1986). Heat sensitivity is increased under pathological condi-

tions such as inherited erythromelalgia, systemic inflammatory disorders, peripheral nerve injuries, chemotherapy-induced neuropathy, and postherpetic neuralgia (Colloca et al., 2017; Ji et al., 2002). Associated were alterations in neuroinflammatory cytokines, neurotrophins, or GABA and glutamatergic transmissions in the spinal cord (Bráz et al., 2015; Gao et al., 2009; Ji et al., 2002; Woolf and Salter, 2000). Mechanical and cold hypersensitivities after injury involves NRG1-ErbB2 signaling in the microglia of spinal dorsal horn (Calvo et al., 2011; Calvo et al., 2010). This study provides evidence for the involvement of NRG1 and ErbB4 in heat hypersensitivity in inflammatory and neuropathic pain. Both NRG1 and pErbB4 are increased in CFA and CCI mice. Heat hypersensitivity in both models is attenuated by neutralizing NRG1 or by inhibiting ErbB4 in the spinal cord. Intrathecal injection of exogenous NRG1 increases heat hypersensitivity in a manner that requires ErbB4 and its kinase activity. Consistently, chemogenetic activation of the ErbB4+ neurons enhanced the responses to noxious heat. Finally, ErbB4+ cells in the spinal cord are positive for NeuN, a marker of neurons, but not for glial markers such as GFAP, Iba1, or Olig2 (data not shown); NRG1 potentiation of heat sensation could be blocked by ErbB4 deletion in rKO mice or inhibition in T796G mice. These results suggest that increased heat sensation by NRG1 is likely to result from increased glutamatergic transmission. However, it is possible that heat hypersensitivity may result from ectopic expression of ErbB4 in cells that do not express ErbB4 under physiological circumstances.

## STAR★METHODS

Detailed methods are provided in the online version of this paper and include the following:

- KEY RESOURCES TABLE
- RESOURCE AVAILABILITY
  - Lead contact
  - Materials availability
  - Data and code availability
- EXPERIMENTAL MODEL AND SUBJECT DETAILS
  - Animals
- METHOD DETAILS
  - Gene expression analysis of noxious heat-activated spinal neurons
  - Tamoxifen treatment
  - Surgical procedures
  - Western blot
  - Immunohistochemistry
  - Fluorescence in situ hybridization (RNAscope)
  - Spinal cord slice preparation
  - Optogenetics and electrophysiological recording in spinal slices
  - Semi-intact preparation and ex vivo recording
  - Dorsal root stimulation
  - Behavioral tests
  - CFA and CCI models
  - Analysis of snRNA-seq data
- QUANTIFICATION AND STATISTICAL ANALYSIS

## SUPPLEMENTAL INFORMATION

Supplemental information can be found online at <https://doi.org/10.1016/j.neuron.2022.04.021>.

## ACKNOWLEDGMENTS

We thank Dr. Cary Lai for the ErbB4 antibody. This work was supported in part by grants from NIH, United States. The graphical abstract was created from BioRender.com.

## AUTHOR CONTRIBUTIONS

L.M., W.-C.X., and H.W. designed the experiments; H.W., W. Chen, and Z.D. conducted experiments, with assistance from G.X., W. Cui, L.Y., W.-J.Z., H.L.R., Y.B., Z.L., K.Z., B.L., N.G., H.Z., X.R., and Z.Y.; H.W., J.M., and L.M. wrote the manuscript.

## DECLARATION OF INTERESTS

The authors declare no competing interests.

Received: August 8, 2021

Revised: March 14, 2022

Accepted: April 19, 2022

Published: May 12, 2022

## REFERENCES

- Abraira, V.E., Kuehn, E.D., Chirila, A.M., Springel, M.W., Toliver, A.A., Zimmerman, A.L., Orefice, L.L., Boyle, K.A., Bai, L., Song, B.J., et al. (2017). The cellular and synaptic architecture of the mechanosensory dorsal horn. *Cell* 168, 295–310.e19.
- Andrew, D., and Craig, A.D. (2001). Spinothalamic lamina I neurons selectively sensitive to histamine: a central neural pathway for itch. *Nat. Neurosci.* 4, 72–77.
- Arcourt, A., Gorham, L., Dhandapani, R., Prato, V., Taberner, F.J., Wende, H., Gangadharan, V., Birchmeier, C., Heppenstall, P.A., and Lechner, S.G. (2017). Touch receptor-derived sensory information alleviates acute pain signaling and fine-tunes nociceptive reflex coordination. *Neuron* 93, 179–193.
- Armbruster, B.N., Li, X., Pausch, M.H., Herlitze, S., and Roth, B.L. (2007). Evolving the lock to fit the key to create a family of G protein-coupled receptors potentially activated by an inert ligand. *Proc. Natl. Acad. Sci. USA* 104, 5163–5168.
- Baba, H., Doubell, T.P., and Woolf, C.J. (1999). Peripheral inflammation facilitates Abeta fiber-mediated synaptic input to the substantia gelatinosa of the adult rat spinal cord. *J. Neurosci.* 19, 859–867.
- Basbaum, A.I., Bautista, D.M., Scherrer, G., and Julius, D. (2009). Cellular and molecular mechanisms of pain. *Cell* 139, 267–284.
- Bean, J.C., Lin, T.W., Sathyamurthy, A., Liu, F., Yin, D.M., Xiong, W.C., and Mei, L. (2014). Genetic labeling reveals novel cellular targets of schizophrenia susceptibility gene: distribution of GABA and non-GABA ErbB4-positive cells in adult mouse brain. *J. Neurosci.* 34, 13549–13566.
- Beaudry, H., Daou, I., Ase, A.R., Ribeiro-da-Silva, A., and Séguéla, P. (2017). Distinct behavioral responses evoked by selective optogenetic stimulation of the major TRPV1+ and MrgD+ subsets of C-fibers. *Pain* 158, 2329–2339.
- Blix, M. (1882). Experimentala bidrag till lösning af fragan om hudnervernas specifika energi. *Uppsala Lakfor Förh* 18, 87–102.
- Bonin, R.P., Bories, C., and De Koninck, Y. (2014). A simplified up-down method (SUDO) for measuring mechanical nociception in rodents using von Frey filaments. *Mol. Pain* 10, 26.
- Bráz, J.M., Wang, X., Guan, Z., Rubenstein, J.L., and Basbaum, A.I. (2015). Transplant-mediated enhancement of spinal cord GABAergic inhibition reverses paclitaxel-induced mechanical and heat hypersensitivity. *Pain* 156, 1084–1091.
- Brenneis, C., Kistner, K., Puopolo, M., Segal, D., Roberson, D., Sisignano, M., Labocha, S., Ferreirós, N., Strominger, A., Cobos, E.J., et al. (2013). Phenotyping the function of TRPV1-expressing sensory neurons by targeted axonal silencing. *J. Neurosci.* 33, 315–326.
- Brenner, D.S., Golden, J.P., and Gereau, R.W.t. (2012). A novel behavioral assay for measuring cold sensation in mice. *PLoS One* 7, e39765.
- Calvo, M., Zhu, N., Grist, J., Ma, Z., Loeb, J.A., and Bennett, D.L. (2011). Following nerve injury neuregulin-1 drives microglial proliferation and neuropathic pain via the MEK/ERK pathway. *Glia* 59, 554–568.
- Calvo, M., Zhu, N., Tsantoulas, C., Ma, Z., Grist, J., Loeb, J.A., and Bennett, D.L. (2010). Neuregulin-ErbB signaling promotes microglial proliferation and chemotaxis contributing to microgliosis and pain after peripheral nerve injury. *J. Neurosci.* 30, 5437–5450.
- Caterina, M.J., Schumacher, M.A., Tominaga, M., Rosen, T.A., Levine, J.D., and Julius, D. (1997). The capsaicin receptor: a heat-activated ion channel in the pain pathway. *Nature* 389, 816–824.
- Cavanaugh, D.J., Chesler, A.T., Bráz, J.M., Shah, N.M., Julius, D., and Basbaum, A.I. (2011). Restriction of transient receptor potential vanilloid-1 to the peptidergic subset of primary afferent neurons follows its developmental downregulation in nonpeptidergic neurons. *J. Neurosci.* 31, 10119–10127.
- Cavanaugh, D.J., Lee, H., Lo, L., Shields, S.D., Zylka, M.J., Basbaum, A.I., and Anderson, D.J. (2009). Distinct subsets of unmyelinated primary sensory fibers mediate behavioral responses to noxious thermal and mechanical stimuli. *Proc. Natl. Acad. Sci. USA* 106, 9075–9080.
- Cervero, F., Bennett, G.J., and Headley, P.M. (1989). Processing of sensory information in the superficial dorsal horn of the spinal cord (Springer).
- Chen, Y.J., Zhang, M., Yin, D.M., Wen, L., Ting, A., Wang, P., Lu, Y.S., Zhu, X.H., Li, S.J., Wu, C.Y., et al. (2010). ErbB4 in parvalbumin-positive interneurons is critical for neuregulin 1 regulation of long-term potentiation. *Proc. Natl. Acad. Sci. USA* 107, 21818–21823.
- Choi, S., Hachisuka, J., Brett, M.A., Magee, A.R., Omori, Y., Iqbal, N.U., Zhang, D., DeLisle, M.M., Wolfson, R.L., Bai, L., et al. (2020). Parallel ascending spinal pathways for affective touch and pain. *Nature* 587, 258–263.
- Christensen, A.J., Iyer, S.M., François, A., Vyas, S., Ramakrishnan, C., Vesuna, S., Deisseroth, K., Scherrer, G., and Delp, S.L. (2016). In vivo interrogation of spinal mechanosensory circuits. *Cell Rep.* 17, 1699–1710.
- Colloca, L., Ludman, T., Bouhassira, D., Baron, R., Dickenson, A.H., Yarnitsky, D., Freeman, R., Truini, A., Attal, N., Finnerup, N.B., et al. (2017). Neuropathic pain. *Nat. Rev. Dis. Primers* 3, 17002.
- Craig, A.D. (2003). Pain mechanisms: labeled lines versus convergence in central processing. *Annu. Rev. Neurosci.* 26, 1–30.
- Craig, A.D., and Bushnell, M.C. (1994). The thermal grill illusion: unmasking the burn of cold pain. *Science* 265, 252–255.
- Dickie, A.C., Bell, A.M., Iwagaki, N., Polgár, E., Gutierrez-Mecinas, M., Kelly, R., Lyon, H., Turnbull, K., West, S.J., Etlin, A., et al. (2019). Morphological and functional properties distinguish the substance P and gastrin-releasing peptide subsets of excitatory interneuron in the spinal cord dorsal horn. *Pain* 160, 442–462.
- Dixon, W.J. (1965). The up-and-down method for small samples. *J. Am. Stat. Assoc.* 60, 967–978.
- Dong, Z., Chen, W., Chen, C., Wang, H., Cui, W., Tan, Z., Robinson, H., Gao, N., Luo, B., Zhang, L., et al. (2020). CUL3 deficiency causes social deficits and anxiety-like behaviors by impairing excitation-inhibition balance through the promotion of cap-dependent translation. *Neuron* 105, 475–490.e6.
- Donnelly, C.R., Jiang, C., Andriessen, A.S., Wang, K., Wang, Z., Ding, H., Zhao, J., Luo, X., Lee, M.S., Lei, Y.L., et al. (2021). STING controls nociception via type I interferon signalling in sensory neurons. *Nature* 591, 275–280.
- Du, J.Y., Price, M.P., Tauger, R.J., Grigsby, D., Ash, J.J., Stark, A.C., Hossain Saad, M.Z.H., Singh, K., Mandal, J., Wemmie, J.A., and Welsh, M.J. (2017). Transient acidosis while retrieving a fear-related memory enhances its lability. *eLife* 6.
- Duan, B., Cheng, L., Bourane, S., Britz, O., Padilla, C., Garcia-Campmany, L., Krashes, M., Knowlton, W., Velasquez, T., Ren, X., et al. (2014). Identification

- of spinal circuits transmitting and gating mechanical pain. *Cell* 159, 1417–1432.
- Eilam, R., Pinkas-Kramarski, R., Ratzkin, B.J., Segal, M., and Yarden, Y. (1998). Activity-dependent regulation of Neu differentiation factor/neuregulin expression in rat brain. *Proc. Natl. Acad. Sci. USA* 95, 1888–1893.
- Emery, E.C., Luiz, A.P., Sikandar, S., Magnúsdóttir, R., Dong, X., and Wood, J.N. (2016). In vivo characterization of distinct modality-specific subsets of somatosensory neurons using GCaMP. *Sci. Adv.* 2, e1600990.
- Fatima, M., Ren, X., Pan, H., Slade, H.F.E., Asmar, A.J., Xiong, C.M., Shi, A., Xiong, A.E., Wang, L., and Duan, B. (2019). Spinal somatostatin-positive interneurons transmit chemical itch. *Pain* 160, 1166–1174.
- Fazzari, P., Paternain, A.V., Valiente, M., Pla, R., Luján, R., Lloyd, K., Lerma, J., Marín, O., and Rico, B. (2010). Control of cortical GABA circuitry development by Nrg1 and ErbB4 signalling. *Nature* 464, 1376–1380.
- Flames, N., Long, J.E., Garratt, A.N., Fischer, T.M., Gassmann, M., Birchmeier, C., Lai, C., Rubenstein, J.L., and Marín, O. (2004). Short- and long-range attraction of cortical GABAergic interneurons by neuregulin-1. *Neuron* 44, 251–261.
- Gao, Y.J., Zhang, L., Samad, O.A., Suter, M.R., Yasuhiko, K., Xu, Z.Z., Park, J.Y., Lind, A.L., Ma, Q., and Ji, R.R. (2009). JNK-induced MCP-1 production in spinal cord astrocytes contributes to central sensitization and neuropathic pain. *J. Neurosci.* 29, 4096–4108.
- García-Rivello, H., Taranda, J., Said, M., Cabeza-Meckert, P., Vila-Petroff, M., Scaglione, J., Ghio, S., Chen, J., Lai, C., Laguens, R.P., et al. (2005). Dilated cardiomyopathy in Erb-b4-deficient ventricular muscle. *Am. J. Physiol. Heart Circ. Physiol.* 289, H1153–H1160.
- Gatto, G., Bourane, S., Ren, X., Di Costanzo, S., Fenton, P.K., Halder, P., Seal, R.P., and Goulding, M.D. (2021). A functional topographic map for spinal sensorimotor reflexes. *Neuron* 109, 91–104.e5.
- Glatzel, M., Flechsig, E., Navarro, B., Klein, M.A., Paterna, J.C., Büeler, H., and Aguzzi, A. (2000). Adenoviral and adeno-associated viral transfer of genes to the peripheral nervous system. *Proc. Natl. Acad. Sci. USA* 97, 442–447.
- Gradwell, M.A., and Abaira, V.E. (2021). Sensory symphonies: how excitatory spinal cord modules orchestrate behavior. *Neuron* 109, 3–5.
- Green, B.G. (2004). Temperature perception and nociception. *J. Neurobiol.* 61, 13–29.
- Gutierrez-Mecinas, M., Bell, A., Polgár, E., Watanabe, M., and Todd, A.J. (2019). Expression of neuropeptide FF defines a population of excitatory interneurons in the superficial dorsal horn of the mouse spinal cord that respond to noxious and pruritic stimuli. *Neuroscience* 416, 281–293.
- Gutierrez-Mecinas, M., Bell, A.M., Marín, A., Taylor, R., Boyle, K.A., Furuta, T., Watanabe, M., Polgár, E., and Todd, A.J. (2017). Preprotachykinin A is expressed by a distinct population of excitatory neurons in the mouse superficial spinal dorsal horn including cells that respond to noxious and pruritic stimuli. *Pain* 158, 440–456.
- Gutierrez-Mecinas, M., Kuehn, E.D., Abaira, V.E., Polgár, E., Watanabe, M., and Todd, A.J. (2016). Immunostaining for Homer reveals the majority of excitatory synapses in laminae I–III of the mouse spinal dorsal horn. *Neuroscience* 329, 171–181.
- Hachisuka, J., Baumbauer, K.M., Omori, Y., Snyder, L.M., Koerber, H.R., and Ross, S.E. (2016). Semi-intact ex vivo approach to investigate spinal somatosensory circuits. *eLife* 5, e22866.
- Hachisuka, J., Koerber, H.R., and Ross, S.E. (2020). Selective-cold output through a distinct subset of lamina I spinoparabrachial neurons. *Pain* 161, 185–194.
- Haenraets, K., Foster, E., Johannssen, H., Kandra, V., Frezel, N., Steffen, T., Jaramillo, V., Paterna, J.C., Zeilhofer, H.U., and Wildner, H. (2017). Spinal nociceptive circuit analysis with recombinant adeno-associated viruses: the impact of serotypes and promoters. *J. Neurochem.* 142, 721–733.
- Han, L., Ma, C., Liu, Q., Weng, H.J., Cui, Y., Tang, Z., Kim, Y., Nie, H., Qu, L., Patel, K.N., et al. (2013). A subpopulation of nociceptors specifically linked to itch. *Nat. Neurosci.* 16, 174–182.
- Han, Q., Kim, Y.H., Wang, X., Liu, D., Zhang, Z.J., Bey, A.L., Lay, M., Chang, W., Berta, T., Zhang, Y., et al. (2016). SHANK3 deficiency impairs heat hyperalgesia and TRPV1 signaling in primary sensory neurons. *Neuron* 92, 1279–1293.
- Han, Z.S., Zhang, E.T., and Craig, A.D. (1998). Nociceptive and thermoreceptive lamina I neurons are anatomically distinct. *Nat. Neurosci.* 1, 218–225.
- Hargreaves, K., Dubner, R., Brown, F., Flores, C., and Joris, J. (1988). A new and sensitive method for measuring thermal nociception in cutaneous hyperalgesia. *Pain* 32, 77–88.
- Häring, M., Zeisel, A., Hochgerner, H., Rinwa, P., Jakobsson, J.E.T., Lönnerberg, P., La Manno, G., Sharma, N., Borgius, L., Kiehn, O., et al. (2018). Neuronal atlas of the dorsal horn defines its architecture and links sensory input to transcriptional cell types. *Nat. Neurosci.* 21, 869–880.
- Hasegawa, H., Abbott, S., Han, B.X., Qi, Y., and Wang, F. (2007). Analyzing somatosensory axon projections with the sensory neuron-specific Advillin gene. *J. Neurosci.* 27, 14404–14414.
- Holmes, W.E., Sliwkowski, M.X., Akita, R.W., Henzel, W.J., Lee, J., Park, J.W., Yansura, D., Abadi, N., Raab, H., and Lewis, G.D. (1992). Identification of heregulin, a specific activator of p185erbB2. *Science* 256, 1205–1210.
- Holstege, J.C., de Graaff, W., Hossaini, M., Cardona Cano, S., Jaarsma, D., van den Akker, E., and Deschamps, J. (2008). Loss of Hoxb8 alters spinal dorsal laminae and sensory responses in mice. *Proc. Natl. Acad. Sci. USA* 105, 6338–6343.
- Huang, J., Polgár, E., Solinski, H.J., Mishra, S.K., Tseng, P.Y., Iwagaki, N., Boyle, K.A., Dickie, A.C., Kriegbaum, M.C., Wildner, H., et al. (2018). Circuit dissection of the role of somatostatin in itch and pain. *Nat. Neurosci.* 21, 707–716.
- Huang, T., Lin, S.H., Malewicz, N.M., Zhang, Y., Zhang, Y., Goulding, M., LaMotte, R.H., and Ma, Q. (2019). Identifying the pathways required for coping behaviours associated with sustained pain. *Nature* 565, 86–90.
- Hunt, S.P., Pini, A., and Evan, G. (1987). Induction of c-fos-like protein in spinal cord neurons following sensory stimulation. *Nature* 328, 632–634.
- Ji, R.R., Samad, T.A., Jin, S.X., Schmolli, R., and Woolf, C.J. (2002). p38 MAPK activation by NGF in primary sensory neurons after inflammation increases TRPV1 levels and maintains heat hyperalgesia. *Neuron* 36, 57–68.
- Julius, D., and Basbaum, A.I. (2001). Molecular mechanisms of nociception. *Nature* 413, 203–210.
- Knowlton, W.M., Palkar, R., Lippoldt, E.K., McCoy, D.D., Baluch, F., Chen, J., and McKemy, D.D. (2013). A sensory-labeled line for cold: TRPM8-expressing sensory neurons define the cellular basis for cold, cold pain, and cooling-mediated analgesia. *J. Neurosci.* 33, 2837–2848.
- Koch, S.C., Acton, D., and Goulding, M. (2018). Spinal circuits for touch, pain, and itch. *Annu. Rev. Physiol.* 80, 189–217.
- Krashes, M.J., Koda, S., Ye, C., Rogan, S.C., Adams, A.C., Cusher, D.S., Maratos-Flier, E., Roth, B.L., and Lowell, B.B. (2011). Rapid, reversible activation of AgRP neurons drives feeding behavior in mice. *J. Clin. Invest.* 121, 1424–1428.
- Krivoshaya, D., Tapia, L., Levinson, J.N., Huang, K., Kang, Y., Hines, R., Ting, A.K., Craig, A.M., Mei, L., Bamji, S.X., and El-Husseini, A. (2008). ErbB4-neuregulin signaling modulates synapse development and dendritic arborization through distinct mechanisms. *J. Biol. Chem.* 283, 32944–32956.
- Li, D., Ambrogio, L., Shimamura, T., Kubo, S., Takahashi, M., Chiriac, L.R., Padera, R.F., Shapiro, G.I., Baum, A., Himmelsbach, F., et al. (2008). BIBW2992, an irreversible EGFR/HER2 inhibitor highly effective in preclinical lung cancer models. *Oncogene* 27, 4702–4711.
- Li, L., Cleary, S., Mandarano, M.A., Long, W.W., Birchmeier, C., and Jones, F.E. (2002). The breast proto-oncogene, HRG alpha regulates epithelial proliferation and lobuloalveolar development in the mouse mammary gland. *Oncogene* 21, 4900–4907.
- Light, A.R., and Perl, E.R. (1979). Spinal termination of functionally identified primary afferent neurons with slowly conducting myelinated fibers. *J. Comp. Neurol.* 186, 133–150.

- Lima, D., and Coimbra, A. (1986). A Golgi study of the neuronal population of the marginal zone (lamina I) of the rat spinal cord. *J. Comp. Neurol.* *244*, 53–71.
- Lin, T.W., Tan, Z., Barik, A., Yin, D.M., Brudvik, E., Wang, H., Xiong, W.C., and Mei, L. (2018). Regulation of synapse development by Vgat deletion from ErbB4-positive interneurons. *J. Neurosci.* *38*, 2533–2550.
- Liu, X., Bates, R., Yin, D.M., Shen, C., Wang, F., Su, N., Kirov, S.A., Luo, Y., Wang, J.Z., Xiong, W.C., et al. (2011). Specific regulation of NRG1 isoform expression by neuronal activity. *J. Neurosci.* *31*, 8491–8501.
- Liu, Y., Latremoliere, A., Li, X., Zhang, Z., Chen, M., Wang, X., Fang, C., Zhu, J., Alexandre, C., Gao, Z., et al. (2018). Touch and tactile neuropathic pain sensitivity are set by corticospinal projections. *Nature* *561*, 547–550.
- Lopez-Garcia, J.A., and King, A.E. (1994). Membrane properties of physiologically classified rat dorsal horn neurons in vitro: correlation with cutaneous sensory afferent input. *Eur. J. Neurosci.* *6*, 998–1007.
- Lu, Y., Sun, X.D., Hou, F.Q., Bi, L.L., Yin, D.M., Liu, F., Chen, Y.J., Bean, J.C., Jiao, H.F., Liu, X., et al. (2014). Maintenance of GABAergic activity by neuregulin 1-ErbB4 in amygdala for fear memory. *Neuron* *84*, 835–846.
- Ma, Q. (2010). Labeled lines meet and talk: population coding of somatic sensations. *J. Clin. Invest.* *120*, 3773–3778.
- Madisen, L., Zwingman, T.A., Sunkin, S.M., Oh, S.W., Zariwala, H.A., Gu, H., Ng, L.L., Palmiter, R.D., Hawrylycz, M.J., Jones, A.R., et al. (2010). A robust and high-throughput Cre reporting and characterization system for the whole mouse brain. *Nat. Neurosci.* *13*, 133–140.
- McCoy, E.S., Taylor-Blake, B., Street, S.E., Pribisko, A.L., Zheng, J., and Zylka, M.J. (2013). Peptidergic CGRP $\alpha$  primary sensory neurons encode heat and itch and tonically suppress sensitivity to cold. *Neuron* *78*, 138–151.
- Mei, L., and Nave, K.A. (2014). Neuregulin-ERBB signaling in the nervous system and neuropsychiatric diseases. *Neuron* *83*, 27–49.
- Mei, L., and Xiong, W.C. (2008). Neuregulin 1 in neural development, synaptic plasticity and schizophrenia. *Nat. Rev. Neurosci.* *9*, 437–452.
- Melzack, R., and Wall, P.D. (1965). Pain mechanisms: a new theory. *Science* *150*, 971–979.
- Merskey, H.E. (1986). Classification of chronic pain. Descriptions of chronic pain syndromes and definitions of pain terms. Prepared by the International Association for the Study of Pain, Subcommittee on Taxonomy. *Pain Suppl.* *3*, S1–S226.
- Meyer, D., and Birchmeier, C. (1995). Multiple essential functions of neuregulin in development. *Nature* *378*, 386–390.
- Michailov, G.V., Sereda, M.W., Brinkmann, B.G., Fischer, T.M., Haug, B., Birchmeier, C., Role, L., Lai, C., Schwab, M.H., and Nave, K.A. (2004). Axonal neuregulin-1 regulates myelin sheath thickness. *Science* *304*, 700–703.
- Moayed, M., and Davis, K.D. (2013). Theories of pain: from specificity to gate control. *J. Neurophysiol.* *109*, 5–12.
- Moritz, A.R., and Henriques, F.C. (1947). Studies of thermal injury: II. The relative importance of time and surface temperature in the causation of cutaneous burns. *Am. J. Pathol.* *23*, 695–720.
- Morris, J.K., Lin, W., Hauser, C., Marchuk, Y., Getman, D., and Lee, K.F. (1999). Rescue of the cardiac defect in ErbB2 mutant mice reveals essential roles of ErbB2 in peripheral nervous system development. *Neuron* *23*, 273–283.
- Müller, J. (1840). *Handbuch der Physiologie des Menschen für Vorlesungen*. J. Hölscher 2.
- Norrrell, U., Finger, S., and Lajonchere, C. (1999). Cutaneous sensory spots and the "law of specific nerve energies": history and development of ideas. *Brain Res. Bull.* *48*, 457–465.
- Olson, W., Abdus-Saboor, I., Cui, L., Burdige, J., Raabe, T., Ma, M., and Luo, W. (2017). Sparse genetic tracing reveals regionally specific functional organization of mammalian nociceptors. *eLife* *6*.
- Pan, H., Fatima, M., Li, A., Lee, H., Cai, W., Horwitz, L., Hor, C.C., Zaher, N., Cin, M., Slade, H., et al. (2019). Identification of a spinal circuit for mechanical and persistent spontaneous itch. *Neuron* *103*, 1135–1149.e6.
- Paricio-Montesinos, R., Schwaller, F., Udhayachandran, A., Rau, F., Walcher, J., Evangelista, R., Vriens, J., Voets, T., Poulet, J.F.A., and Lewin, G.R. (2020). The sensory coding of warm perception. *Neuron* *106*, 830–841.e3.
- Peirs, C., and Seal, R.P. (2016). Neural circuits for pain: recent advances and current views. *Science* *354*, 578–584.
- Perl, E.R. (2007). Ideas about pain, a historical view. *Nat. Rev. Neurosci.* *8*, 71–80.
- Petreaanu, L., Mao, T., Sternson, S.M., and Svoboda, K. (2009). The subcellular organization of neocortical excitatory connections. *Nature* *457*, 1142–1145.
- Pogorzala, L.A., Mishra, S.K., and Hoon, M.A. (2013). The cellular code for mammalian thermosensation. *J. Neurosci.* *33*, 5533–5541.
- Polgár, E., Sardella, T.C.P., Tiong, S.Y.X., Locke, S., Watanabe, M., and Todd, A.J. (2013). Functional differences between neurochemically defined populations of inhibitory interneurons in the rat spinal dorsal horn. *Pain* *154*, 2606–2615.
- Prescott, S.A., Ma, Q., and De Koninck, Y. (2014). Normal and abnormal coding of somatosensory stimuli causing pain. *Nat. Neurosci.* *17*, 183–191.
- Ramirez, S., Liu, X., Lin, P.A., Suh, J., Pignatelli, M., Redondo, R.L., Ryan, T.J., and Tonegawa, S. (2013). Creating a false memory in the hippocampus. *Science* *341*, 387–391.
- Reijmers, L.G., Perkins, B.L., Matsuo, N., and Mayford, M. (2007). Localization of a stable neural correlate of associative memory. *Science* *317*, 1230–1233.
- Riethmacher, D., Sonnenberg-Riethmacher, E., Brinkmann, V., Yamaai, T., Lewin, G.R., and Birchmeier, C. (1997). Severe neuropathies in mice with targeted mutations in the ErbB3 receptor. *Nature* *389*, 725–730.
- Robinson, H.L., Tan, Z., Santiago-Marrero, I., Arzola, E.P., Dong, T.V., Xiong, W.C., and Mei, L. (2022). Neuregulin 1 and ErbB4 kinase actively regulate sharp wave ripples in the hippocampus. *J. Neurosci.* *42*, 390–404.
- Rodriguez, E., Sakurai, K., Xu, J., Chen, Y., Toda, K., Zhao, S., Han, B.X., Ryu, D., Yin, H., Liedtke, W., and Wang, F. (2017). A craniofacial-specific monosynaptic circuit enables heightened affective pain. *Nat. Neurosci.* *20*, 1734–1743.
- Rottkamp, C.A., Lobur, K.J., Wladyka, C.L., Lucky, A.K., and O’Gorman, S. (2008). Pbx3 is required for normal locomotion and dorsal horn development. *Dev. Biol.* *314*, 23–39.
- Russ, D.E., Cross, R.B.P., Li, L., Koch, S.C., Matson, K.J.E., Yadav, A., Alkaslasi, M.R., Lee, D.I., Le Pichon, C.E., Menon, V., and Levine, A.J. (2021). A harmonized atlas of mouse spinal cord cell types and their spatial organization. *Nat. Commun.* *12*, 5722.
- Shamir, A., Kwon, O.B., Karavanova, I., Vullhorst, D., Leiva-Salcedo, E., Janssen, M.J., and Buonanno, A. (2012). The importance of the NRG1/ErbB4 pathway for synaptic plasticity and behaviors associated with psychiatric disorders. *J. Neurosci.* *32*, 2988–2997.
- Sharif, B., Ase, A.R., Ribeiro-da-Silva, A., and Séguéla, P. (2020). Differential coding of itch and pain by a subpopulation of primary afferent neurons. *Neuron* *106*, 940–951.e4.
- Stemkowski, P., Garcia-Caballero, A., De Maria Gadotti, V., M’Dahoma, S., Huang, S., Gertrud Black, S.A., Chen, L., Souza, I.A., Zhang, Z., and Zamponi, G.W. (2017). TRPV1 nociceptor activity initiates USP5/T-type channel-mediated plasticity. *Cell Rep.* *18*, 2289–2290.
- Sun, Y.G., Zhao, Z.Q., Meng, X.L., Yin, J., Liu, X.Y., and Chen, Z.F. (2009). Cellular basis of itch sensation. *Science* *325*, 1531–1534.
- Szabo, N.E., da Silva, R.V., Sotocinal, S.G., Zeilhofer, H.U., Mogil, J.S., and Kania, A. (2015). Hoxb8 intersection defines a role for Lmx1b in excitatory dorsal horn neuron development, spinofugal connectivity, and nociception. *J. Neurosci.* *35*, 5233–5246.
- Tan, G.H., Liu, Y.Y., Hu, X.L., Yin, D.M., Mei, L., and Xiong, Z.Q. (2011). Neuregulin 1 represses limbic epileptogenesis through ErbB4 in parvalbumin-expressing interneurons. *Nat. Neurosci.* *15*, 258–266.
- Tan, Z., Robinson, H.L., Yin, D.M., Liu, Y., Liu, F., Wang, H., Lin, T.W., Xing, G., Gan, L., Xiong, W.C., and Mei, L. (2018). Dynamic ErbB4 activity in

- hippocampal-prefrontal synchrony and top-down attention in rodents. *Neuron* 98, 380–393.e4.
- Taveggia, C., Zanazzi, G., Petrylak, A., Yano, H., Rosenbluth, J., Einheber, S., Xu, X., Esper, R.M., Loeb, J.A., Shrager, P., et al. (2005). Neuregulin-1 type III determines the ensheathment fate of axons. *Neuron* 47, 681–694.
- Taves, S., Berta, T., Liu, D.L., Gan, S., Chen, G., Kim, Y.H., Van de Ven, T., Laufer, S., and Ji, R.R. (2016). Spinal inhibition of p38 MAP kinase reduces inflammatory and neuropathic pain in male but not female mice: sex-dependent microglial signaling in the spinal cord. *Brain Behav. Immun.* 55, 70–81.
- Thunberg, T. (1896). Förmimelserna vid till samma Ställe lokaliserad, samtidigt pågående köld-och värmeretning. *Uppsala Läkfören Förh* 2, 489–495.
- Tidcombe, H., Jackson-Fisher, A., Mathers, K., Stern, D.F., Gassmann, M., and Golding, J.P. (2003). Neural and mammary gland defects in ErbB4 knockout mice genetically rescued from embryonic lethality. *Proc. Natl. Acad. Sci. USA* 100, 8281–8286.
- Ting, A.K., Chen, Y., Wen, L., Yin, D.M., Shen, C., Tao, Y., Liu, X., Xiong, W.C., and Mei, L. (2011). Neuregulin 1 promotes excitatory synapse development and function in GABAergic interneurons. *J. Neurosci.* 31, 15–25.
- Todd, A.J. (2010). Neuronal circuitry for pain processing in the dorsal horn. *Nat. Rev. Neurosci.* 11, 823–836.
- Tominaga, M., Caterina, M.J., Malmberg, A.B., Rosen, T.A., Gilbert, H., Skinner, K., Raumann, B.E., Basbaum, A.I., and Julius, D. (1998). The cloned capsaicin receptor integrates multiple pain-producing stimuli. *Neuron* 21, 531–543.
- Tricoire, L., Pelkey, K.A., Daw, M.I., Sousa, V.H., Miyoshi, G., Jeffries, B., Cauli, B., Fishell, G., and McBain, C.J. (2010). Common origins of hippocampal lvy and nitric oxide synthase expressing neurogliaform cells. *J. Neurosci.* 30, 2165–2176.
- Velanac, V., Unterbarnscheidt, T., Hinrichs, W., Gummert, M.N., Fischer, T.M., Rossner, M.J., Trimarco, A., Brivio, V., Taveggia, C., Willem, M., et al. (2012). Bace1 processing of NRG1 type III produces a myelin-inducing signal but is not essential for the stimulation of myelination. *Glia* 60, 203–217.
- Vriens, J., Nilius, B., and Voets, T. (2014). Peripheral thermosensation in mammals. *Nat. Rev. Neurosci.* 15, 573–589.
- Vullhorst, D., Neddens, J., Karavanova, I., Tricoire, L., Petralia, R.S., McBain, C.J., and Buonanno, A. (2009). Selective expression of ErbB4 in interneurons, but not pyramidal cells, of the rodent hippocampus. *J. Neurosci.* 29, 12255–12264.
- Wang, F., Bélanger, E., Côté, S.L., Desrosiers, P., Prescott, S.A., Côté, D.C., and De Koninck, Y. (2018a). Sensory afferents use different coding strategies for heat and cold. *Cell Rep.* 23, 2001–2013.
- Wang, H., Liu, F., Chen, W., Sun, X., Cui, W., Dong, Z., Zhao, K., Zhang, H., Li, H., Xing, G., et al. (2018b). Genetic recovery of ErbB4 in adulthood partially restores brain functions in null mice. *Proc. Natl. Acad. Sci. U. S. A.* 115, 13105–13110.
- Wang, H.S., Cui, W.P., Chen, W.B., Liu, F., Dong, Z.Q., Xing, G.L., Luo, B., Gao, N.N., Zou, W.J., Zhao, K., et al. (2021). The laterodorsal tegmentum-ventral tegmental area circuit controls depression-like behaviors by activating ErbB4 in DA neurons. *Mol. Psychiatry*, 1–19.
- Wang, X., Zhang, J., Eberhart, D., Urban, R., Meda, K., Solorzano, C., Yamanaka, H., Rice, D., and Basbaum, A.I. (2013). Excitatory superficial dorsal horn interneurons are functionally heterogeneous and required for the full behavioral expression of pain and itch. *Neuron* 78, 312–324.
- Wang, Z.L., Jiang, C.Y., He, Q.R., Matsuda, M., Han, Q.J., Wang, K.Y., Bang, S.S., Ding, H.P., Ko, M.C., and Ji, R.R. (2020). Anti-PD-1 treatment impairs opioid antinociception in rodents and nonhuman primates. *Sci. Transl. Med.* 12.
- Wen, L., Lu, Y.S., Zhu, X.H., Li, X.M., Woo, R.S., Chen, Y.J., Yin, D.M., Lai, C., Terry, A.V., Jr., Vazdarjanova, A., et al. (2010). Neuregulin 1 regulates pyramidal neuron activity via ErbB4 in parvalbumin-positive interneurons. *Proc. Natl. Acad. Sci. USA* 107, 1211–1216.
- Wercberger, R., Braz, J.M., Weinrich, J.A., and Basbaum, A.I. (2021). Pain and itch processing by subpopulations of molecularly diverse spinal and trigeminal projection neurons. *Proc. Natl. Acad. Sci. USA* 118.
- Willem, M., Garratt, A.N., Novak, B., Citron, M., Kaufmann, S., Rittger, A., DeStrooper, B., Saftig, P., Birchmeier, C., and Haass, C. (2006). Control of peripheral nerve myelination by the beta-secretase BACE1. *Science* 314, 664–666.
- Woo, R.S., Li, X.M., Tao, Y., Carpenter-Hyland, E., Huang, Y.Z., Weber, J., Neiswender, H., Dong, X.P., Wu, J., Gassmann, M., et al. (2007). Neuregulin-1 enhances depolarization-induced GABA release. *Neuron* 54, 599–610.
- Woolf, C.J., and Salter, M.W. (2000). Neuronal plasticity: increasing the gain in pain. *Science* 288, 1765–1769.
- Wu, Z., Autry, A.E., Bergan, J.F., Watabe-Uchida, M., and Dulac, C.G. (2014). Galanin neurons in the medial preoptic area govern parental behaviour. *Nature* 509, 325–330.
- Xu, Y., Lopes, C., Wende, H., Guo, Z., Cheng, L., Birchmeier, C., and Ma, Q. (2013). Ontogeny of excitatory spinal neurons processing distinct somatic sensory modalities. *J. Neurosci.* 33, 14738–14748.
- Yao, L.L., Hu, J.X., Li, Q., Lee, D., Ren, X., Zhang, J.S., Sun, D., Zhang, H.S., Wang, Y.G., Mei, L., et al. (2020). Astrocytic neogenin/netrin-1 pathway promotes blood vessel homeostasis and function in mouse cortex. *J. Clin. Invest.* 130, 6490–6509.
- Yao, Z., van Velthoven, C.T.J., Nguyen, T.N., Goldy, J., Sedeno-Cortes, A.E., Baftizadeh, F., Bertagnolli, D., Casper, T., Chiang, M., Crichton, K., et al. (2021). A taxonomy of transcriptomic cell types across the isocortex and hippocampal formation. *Cell* 184, 3222–3241.e26.
- Zeng, H., Gragerov, A., Hohmann, J.G., Pavlova, M.N., Schimpf, B.A., Xu, H., Wu, L.J., Toyoda, H., Zhao, M.G., Rohde, A.D., et al. (2006). Neuromedin U receptor 2-deficient mice display differential responses in sensory perception, stress, and feeding. *Mol. Cell. Biol.* 26, 9352–9363.
- Zhu, X.J., Lai, C., Thomas, S., and Burden, S.J. (1995). Neuregulin receptors, ErbB3 and ErbB4, are localized at neuromuscular synapses. *EMBO J.* 14, 5842–5848.

STAR★METHODS

KEY RESOURCES TABLE

REAGENT or RESOURCE	SOURCE	IDENTIFIER
<b>Antibodies</b>		
rabbit anti-ErbB4 (0618, recognizing residues 1108-1136)	Dr. Cary Lai; <a href="#">Zhu et al., 1995</a>	N/A
rabbit anti-p-ErbB4	Cell Signaling Technology	# 4757; RRID: AB_2099987
mouse anti-β-actin	Cell Signaling Technology	# 3700; RRID:AB_2242334
mouse anti-GAPDH	Cell Signaling Technology	# 97166; RRID:AB_2756824
mouse anti-c-Fos	Santa Cruz	# 71243; RRID:AB_10610067
rabbit anti-c-Fos	Millipore	# ABE457; RRID:AB_2631318
chicken anti-GFP	Aves	# 1020; RRID:AB_10000240
rabbit anti-RFP	Rockland	# 600-401-379-RTU; RRID:AB_2209751
rabbit anti-NeuN	Biosensis	# R-37770-100; RRID:AB_2493045
Alexa-647 conjugated streptavidin	Life technologies	# S21374
<b>Bacterial and Virus Strains</b>		
AAV1-Ef1α-lox-mCherry-lox(dtA)-lox2	UNC vector core	N/A
AAV5-Ef1a-DIO-hChR2(H134R)-EYFP-WPRE-pA	UNC vector core	N/A
AAV5-hSyn-DIO-hM3D(Gq)-mCherry	<a href="#">Krashes et al., 2011</a>	Addgene viral prep # 44361-AAV5; RRID:Addgene_44361
AAV5-hSyn-DIO-hM4D(Gi)-mCherry	<a href="#">Krashes et al., 2011</a>	Addgene viral prep # 44362-AAV5; RRID:Addgene_44362
AAV5-Ef1a-mCherry	Karl Deisseroth (unpublished)	Addgene viral prep # 114470-AAV5; RRID:Addgene_114470
AAV5-hSyn-DIO-mCherry	Bryan Roth (unpublished)	Addgene viral prep # 50459-AAV5; RRID:Addgene_50459
AAV5-hSyn-GFP-Cre	UNC vector core	N/A
AAV5-hSyn-EYFP	UNC vector core	N/A
<b>Chemicals, Peptides, and Recombinant Proteins</b>		
NRG1 (rHRG β, residues 177-244)	Dr. Mark Sliwkowski; <a href="#">Holmes et al., 1992</a>	N/A
1NMPP1	EMD Millipore	# 529581
afatinib	Selleck Chemicals	# S1011
capsaicin	Sigma	# M2028
Complete Freund's Adjuvant (CFA)	Sigma	# F5881
NRG1 beta-1 ELISA Kit	ThermoFisher	# EHNRG1
Clozapine-N-oxide (CNO)	Sigma	# C0832
<b>Deposited Data</b>		
Raw data of single nuclei RNA sequencing (snRNA seq) of spinal cords from adult mice	<a href="#">Russ et al., 2021</a>	GEO # GSE158380
<b>Experimental Models: Organisms/Strains</b>		
Mouse: ErbB4-2A-CreER; B6.Cg- <i>ErbB4</i> <sup>tm1.1(cre/ERT2)Aibs/J</sup>	Jackson Laboratory	RRID:IMSR_JAX:012360
Mouse: Ai9; B6;129S6-Gt( <i>ROSA</i> ) <i>26Sor</i> <sup>tm9(CAG-tdTomato)Hze/J</sup>	Jackson Laboratory	RRID:IMSR_JAX:007905
Mouse: cFos-shEGFP; B6.Cg-Tg(Fos-tTA,Fos-EGFP*)1Mmay/J	Jackson Laboratory	RRID:IMSR_JAX:018306
Mouse: MrgprD-CreER; <i>MrgprD</i> <sup>tm1.1(cre/ERT2)Wql/J</sup>	Jackson Laboratory	RRID:IMSR_JAX:031286

(Continued on next page)

**Continued**

REAGENT or RESOURCE	SOURCE	IDENTIFIER
Mouse: SST-Cre: <i>Sst<sup>tm2.1(cre)Zjh</sup>/J</i>	Jackson Laboratory	RRID:IMSR_JAX:013044
Mouse: CCK-Cre: <i>Cck<sup>tm1.1(cre)Zjh</sup>/J</i>	Jackson Laboratory	RRID:IMSR_JAX:012706
Mouse: Rosa-LSL-EYFP: B6.129X1-Gt( <i>ROSA</i> )26So <sup>tm1(EYFP)Cos</sup> /J	Jackson Laboratory	RRID:IMSR_JAX:006148
Mouse: advillin-CreER: Tg( <i>Avil-icre/ERT2</i> )AJwo/J	Jackson Laboratory	RRID:IMSR_JAX:032027
Mouse: TRPV1-Cre mice: B6.129- <i>Trpv1<sup>tm1(cre)Bbm</sup>/J</i>	Jackson Laboratory	RRID:IMSR_JAX:017769
Mouse: ErbB4f/f: B6.129-ErbB4 <sup>tm1Htig</sup>	Dr. Cecilia M. Hertig; Garcia-Rivello et al., 2005	N/A
Mouse: $\alpha$ MHC::ErbB4	Dr. Jon Golding; Tidcombe et al., 2003	N/A
Mouse: NRG1f/f	Dr. Frank Jones; Li et al., 2002	N/A
Mouse: T796G	Tan et al., 2018	N/A
Mouse: stop-ErbB4	Wang et al., 2018b	N/A

**Software and Algorithms**

Graphpad Prism 6.0	GraphPad Software	<a href="https://www.graphpad.com">https://www.graphpad.com</a>
RStudio	RStudio	<a href="https://www.rstudio.com">https://www.rstudio.com</a>
Cell Ranger	10 x Genomics	<a href="https://support.10xgenomics.com">https://support.10xgenomics.com</a>
pClamp 11	Molecular Devices	<a href="https://www.moleculardevices.com/">https://www.moleculardevices.com/</a>
ImageJ	National Institute of Health	<a href="https://imagej.nih.gov/ij/download.html">https://imagej.nih.gov/ij/download.html</a>
Zen system	Zeiss	<a href="https://www.zeiss.com/microscopy/us/products">https://www.zeiss.com/microscopy/us/products</a>

**RESOURCE AVAILABILITY**

**Lead contact**

For further information and requests, please direct all inquiries to Dr. Lin Mei ([lin.mei@case.edu](mailto:lin.mei@case.edu)).

**Materials availability**

This study did not generate new unique reagents.

**Data and code availability**

SnRNA Seq data in the present study is a re-analysis of raw data from (Russ et al., 2021), original data and associated code are available at <https://www.ncbi.nlm.nih.gov/geo/query/acc.cgi?acc=GSE158380> and <https://github.com/ArielLevineLabNINDS>. Other data reported in this paper will be shared by the lead contact upon request.

This paper does not report original code.

Any additional information required to reanalyze the data reported in this work paper is available from the **Lead Contact** upon request.

**EXPERIMENTAL MODEL AND SUBJECT DETAILS**

**Animals**

ErbB4-2A-CreERT2 mice (#012360), Ai9 (Rosa-CAG-LSL-tdTomato) reporter mice (#007905), cFos::shEGFP mice (#018306), MrgprD-CreER (#031286), SST-Cre (#013044), CCK-Cre (#012706), Rosa-LSL-EYFP (#006148), Advillin-CreER (#032027) and TRPV1-Cre mice (#017769) were obtained from the Jackson Laboratory. ErbB4f/f mice,  $\alpha$ MHC::ErbB4 mice, NRG1f/f, T796G, and stop-ErbB4 mice have been described previously (Garcia-Rivello et al., 2005; Li et al., 2002; Tidcombe et al., 2003; Wang et al., 2018b; Wang et al., 2021). Mice were housed in an environment of 22  $\pm$  2°C and 12 hr light/dark cycle with food and water *ad libitum*. Animal experimental procedures were approved by the Institutional Animal Care and Use Committee of Case Western Reserve University. Male mice were used in the present study. For the recording of A $\beta$ , A $\delta$  and C inputs, 20-30 day-old mice were used. For semi-intact recordings, 4-7 week-old mice were used. For recording in spinal cord slices, viral injections were performed in 2-4 week-old mice and recordings were performed 2-3 weeks later. For behavioral studies, mice of 2-5 month-old were used. Experimenters were blinded to genotypes and treatments.

## METHOD DETAILS

### Gene expression analysis of noxious heat-activated spinal neurons

To reveal gene expression profiles of noxious heat-responsive neurons, cFos::shEGFP mice were subjected to heat stimulation as described previously (Hunt et al., 1987). Briefly, mice were exposed to 52°C hot plate for 10 times with 90-s interval. Heat plate exposure was terminated when mice showed foot withdrawal or licking, or for maximal 20 s to avoid tissue damage. Two hours after the final exposure, mice were perfused with 4% PFA; transverse spinal cord sections (60- $\mu$ m thickness) of the lumbar enlargement were prepared with cryostat. Expression of EGFP and cFos was analyzed by staining with anti-GFP and anti-cFos antibodies. Mice were also perfused with ice-cold sectioning solution (see electrophysiological recording below). Laminae I and II of the lumbar enlargement were identified under microscope based on thickness (referred to the Allen Brain Atlas) and the translucency of lamina II (substantia gelatinosa). Cytoplasm of EGFP+ cells in spinal cord sections were collected by glass pipettes and subjected to reverse transcription using a kit (SuperScript® III CellsDirect, Invitrogen). cDNA was subjected to 2 rounds of PCR as previously described (Tricoire et al., 2010). The first PCR reaction used 1<sup>st</sup>-round primers for all target genes. Resulting products were used as templates for the second PCR reaction with primers for an individual gene (Table S1). Notice that the products of the second PCR were a fragment within the templates generated by the first PCR reaction.

### Tamoxifen treatment

Tamoxifen treatment was performed as previously described with slight modifications (Bean et al., 2014). Tamoxifen was dissolved in ethanol (20 mg/ml) by vortex for 5-10 min. The solution was aliquoted into 1.5-ml tube and equal volume of corn oil was added. The solution was incubated at 60°C for about 1 hr for ethanol to evaporate and stored at -20°C until use. Tamoxifen was administered intraperitoneally (100 mg/kg body weight) once for analysis of somatodendritic morphology, and once every three days, 5 times total for other assays.

### Surgical procedures

Mice were anesthetized with isoflurane; fur covering relevant areas were shaved.

### Fluorogold-based retrograde tracing

Fluorogold was injected as previously described (Wang et al., 2021). Coordinates for injection regions were PAG (AP = -4.4, ML = -0.45, DV = -2.6 mm), LPB (AP = -5.3, ML = -1.25, DV = -3.35 mm), NTS (AP = -6.8, ML = -0.65, DV = -4.4 mm), CVLM (AP = -7.5, ML = -1.3, DV = -4.2 mm), thalamus (AP = -1.75 and 3.3, ML = -0.96, DV = -3.1 and -2.9 mm). Fluorogold (100 nl) was delivered via a glass pipette via a 2.5  $\mu$ l Hamilton syringe (20 nl/min by a MicroSyringe Pump, World Precision Instruments). The pipette was left at injection sites for 5 min before withdrawal. Imaging was performed 4-5 days after injection.

### Intraspinal injection

Intraspinal injection was performed as described previously (Huang et al., 2018). Vertebrae T12-L1 (corresponding to spinal segments L3-L5) were exposed and fixed on a stereotaxic frame. Holes were drilled through the lamina of T13, one on each side, and the dura was perforated by a needle (30 G, 500  $\mu$ m lateral to the vertebrate spine) to avoid damaging underlying spinal cord. AAV was delivered via a glass pipette that was connected to a 2.5  $\mu$ l Hamilton syringe at a rate of 40 nl/min, under control of a MicroSyringe Pump (World Precision Instruments, Sarasota, USA). Dorsal horns of both sides were injected through the space between vertebrae T12/T13 and between T13/L1, and via the holes. Injection volume was 400 or 600 nl and the depth was at 200~300  $\mu$ m below the spinal cord surface. To reduce leakage, the pipettes were left at place for 5 min before withdrawal.

### Intra-DRG injection

Intra-DRG injection was performed as previously described (Glatzel et al., 2000). The L4 and L5 vertebrae was exposed by a 2-cm longitudinal incision and removal of multifidus and longissimus lumborum muscles. The processus accessorius and parts of the processus transversus on the left side were removed to expose the L4/L5 DRGs. The spinal column was fixed in a stereotaxic frame; AAV (300 nl for each DRG) was injected at 30 nl/min via a 36 G NanoFil needle on NanoFil syringe controlled by a micropump (World Precision Instruments, Sarasota, USA).

### Intrathecal injection

Intrathecal injection was performed as previously described (Donnelly et al., 2021). To minimize the stress of surgery, mice were shaved in the region at vertebral levels of L5 and L6 one day before the injection. For the injection, anesthetized mice were placed on a cylinder to better expose the shaved area. NRG1, 1NMPP1, ecto-ErbB4, or afatinib (8  $\mu$ l) was injected into the subdural space via a needle (30 G) inserted into the groove between L5 and L6. Tail flick may be observed to indicate successful needle entry into subdural space. Drug delivery rate (30 s for 8  $\mu$ l) was controlled by a micropump (World Precision instruments, Sarasota, USA).

### Western blot

Western blot was performed as previously reported (Dong et al., 2020). Lumbar enlargement segments of the spinal cord were dissected and the dorsal and ventral horns were carefully separated under a stereo microscope. Tissues were homogenized by sonication in RIPA buffer containing protease inhibitors. Debris was cleared by centrifugation at 12,000 g for 10 min at 4°C. Samples were resolved on SDS-PAGE and transferred to nitrocellulose membranes, which were incubated in PBS (phosphate buffered saline) containing 0.1% Tween-20 and 5% BSA for 1 hr at room temperature (RT) before overnight primary antibody incubation at 4°C. After

wash, membranes were incubated with HRP-conjugated secondary antibody in PBS for 1 hr at RT. After incubating with enhanced chemiluminescence, immunoreactive bands were visualized by LI-COR Odyssey infrared imaging system. Intensity of immunoreactive bands were quantitated with ImageJ (NIH), with  $\beta$ -actin or GAPDH as loading control. The following primary antibodies were used: rabbit anti-ErbB4 (#0618, 1:2,000, generously provided by Dr. Cary Lai) (Zhu et al., 1995), rabbit anti-p-ErbB4 (#4757, 1:200, Cell Signaling Technology), mouse anti- $\beta$ -actin (#3700, 1:5,000, Cell Signaling Technology), and mouse anti-GAPDH (#97166 1:5,000, Cell Signaling Technology).

### Immunohistochemistry

Immunohistochemistry was performed as previously described (Lin et al., 2018). Mice were transcardially perfused with 4% PFA in PBS and the spinal cord were stored in 1% PFA at 4°C overnight. Samples were transferred to 20% and 30% sucrose solution for dehydration at 4°C and embedded with O.C.T medium (Fisher Healthcare). Frozen blocks were cut with cryostat (ThermoFisher, USA) or vibratome (Leica, VT1000 S) to prepare 20–60  $\mu$ m-thick transverse slices. For somatodendritic analysis of ErbB4+ cells, 400- $\mu$ m thick slices were prepared. Slices were washed with PBS and blocked with PBS containing 0.5% Triton-100 and 10% donkey serum for 1 hr at RT, before overnight incubation of primary antibodies at 4°C. After wash, slices were incubated in AlexaFluor secondary antibodies (Jackson ImmunoResearch) for 2 hr at RT. Slices were washed, mounted onto slides and covered with SlowFade Diamond Antifade Mountant (catalog #S36972; Thermo Fisher). The following primary antibodies were used for immunostaining: mouse anti-c-Fos (#271243, 1:500; Santa Cruz), rabbit anti-c-Fos (#ABE457, Millipore), chicken anti-GFP (#1020, 1:1,000, Aves), anti-RFP (#600-401-379-RTU, 1:500, Rockland), and rabbit anti-NeuN (#R-3770-100, 1:500, Biosensis). Alexa-647 conjugated streptavidin (#S21374, 1:200, Life technologies) was used for visualization of biocytin.

### Fluorescence in situ hybridization (RNAscope)

RNAscope was performed as previously described (Liu et al., 2011; Yao et al., 2020). Mice were transcardially perfused with 4% PFA in PBS; isolated spinal cords were stored in 1% PFA at 4°C overnight, transferred to 20% and 30% sucrose solution for dehydration at 4°C until tissues sank to the bottom and embedded with O.C.T medium (Fisher Healthcare). Frozen blocks were sliced by a cryostat (ThermoFisher, USA) into 12  $\mu$ m-thick transverse slices which were mounted onto Super Frost Plus slides. Slices were dehydrated with ethanol, incubated in retrieval buffer at a boiling temperature for 15 min, rinsed in deionized water, and immediately treated with protease at 40°C for 30 min. After washing, the slides were treated with pre-amplifier and amplifier buffers for 30 and 15 min, respectively at 40°C. RNAs were labeled with Opal™ 520 or 570 and imaged under confocal microscope. For some analyses, immunostaining of tdTomato was performed after RNAscope analysis. Probes were purchased from Advanced Cell Diagnostics: Mm-Tacr1, 428781; Mm-Tac1, 410351; Mm-Nmur2, 314111.

### Spinal cord slice preparation

Spinal cord slices were prepared as previously described (Duan et al., 2014; Stenkowski et al., 2017). Mice were anesthetized with isoflurane, and the spinal column including vertebrae and the spinal cord was collected and placed in ice-cold sectioning solution (in mM, 120 Choline-Cl, 2.5 KCl, 0.5 CaCl<sub>2</sub>, 7 MgCl<sub>2</sub>, 1.25 NaH<sub>2</sub>PO<sub>4</sub>, 26 NaHCO<sub>3</sub>, 25 glucose, 1.3 sodium ascorbate and 3.0 sodium pyruvate) oxygenated with 95% O<sub>2</sub> and 5% CO<sub>2</sub>. The lumbar enlargement of the spinal cord was dissected and glued to an agar block (4% low melting agarose). Transverse (400- $\mu$ m) and longitudinal (480- $\mu$ m) sections were prepared with Vibratome (VT1200S, Leica) and were used for recording neuron firing and for afferent input analysis. Slices were incubated in ACSF (in mM, 124 NaCl, 2.5 KCl, 2.5 CaCl<sub>2</sub>, 2 MgCl<sub>2</sub>, 1.25 NaH<sub>2</sub>PO<sub>4</sub>, 26 NaHCO<sub>3</sub>, 10 glucose, 1.3 sodium ascorbate, and 3.0 sodium pyruvate) oxygenated with 95% O<sub>2</sub> and 5% CO<sub>2</sub> at 33°C for 40 min and then at RT for one additional hour. Slices were transferred to a recording chamber and superfused with oxygenated ACSF at a rate of 5 ml/min during recording.

### Optogenetics and electrophysiological recording in spinal slices

Optogenetic study was performed as previously described (Tan et al., 2018) with minor modifications. Spinal slices were placed under an upright microscope (Olympus, BX51WI, Japan) equipped with 10x / 40x water immersion lens (BX51WI, Olympus) and infrared-sensitive CCD camera (C2400-75, Hamamatsu). Optic fibers of 200- $\mu$ m core diameter (Thorlabs, 0.39 NA) were connected to a DHOM laser source (473 nm, 150 mW) for optogenetic stimulation of ChR2. Light power was measured by a power meter (Thorlab, USA) and intensities were calibrated to 0.25 mW/mm<sup>2</sup> for activation of dissociated DRG neurons and 12 mW/mm<sup>2</sup> for activation at spinal cord slices.

Whole-cell patch clamp recording was performed as previously described (Tan et al., 2018). Glass pipettes with resistance of 3–8 M $\Omega$  were prepared with a horizontal puller (Sutter, USA) and filled with internal solution (in mM, 125 K-gluconate, 5 KCl, 10 HEPES, 0.2 EGTA, 1 MgCl<sub>2</sub>, 4 Mg-ATP, 0.3 Na-GTP, 10 phosphocreatine, pH 7.25, 290–300 mOsm). For recording of downstream neurons of ErbB4+ neurons, internal solution (in mM, 125 CsCH<sub>3</sub>SO<sub>3</sub>, 5 CsCl, 10 HEPES, 0.2 EGTA, 1 MgCl<sub>2</sub>, 4 Mg-ATP, 0.3 Na-GTP, 10 phosphocreatine and 0.5% biocytin, pH 7.25, 290–300 mOsm) was used. Data were acquired with MultiClamp 700B amplifier and Digidata 1550A (Molecular Devices). Responses were low-pass filtered on-line at 3 kHz, digitized at 10 kHz.

Resting membrane potential was designated as the membrane potential 10 s after switching from voltage-clamp to current-clamp. To determine the firing patterns, ErbB4+ neurons were held at resting membrane potentials and injected with step currents

(1-s duration, 20 pA increments, delivered every 6 s, ranging from +20 pA to +60 pA). Classification of firing patterns followed the criteria established by previous studies (Cervero et al., 1989; Han et al., 1998; Lima and Coimbra, 1986).

In some experiments, DRGs were prepared as previously reported (Beaudry et al., 2017). Briefly dissected from adult AAV-ChR2-injected TRPV1-Cre mice, digested with dispase and collagenase type II, and mechanically triturated and plated onto 35 mm dishes coated with laminin and poly-D-lysine. After incubation for 4 hr, they were recorded for evoked APs and photocurrents by 473-nm light stimulation.

In study of the effects of NRG1 and afatinib on glutamatergic transmission, optically evoked EPSCs were recorded in neurons downstream to ErbB4+ neurons. They were identified based on the characteristics of evoked EPSCs - constant and short latency ( $\leq 10$  ms) and no failure of induction. To stably induce EPSCs, light intensity that induces EPSC of half-maximal amplitude (LI50) was predetermined. The LI50 was individually identified for each cell. Under illumination of light at LI50 (0.1 Hz), baseline of EPSCs were recorded, followed by recording 15 min after superfusion of NRG1 or afatinib. EPSCs were also recorded 15 min after washout.

### Semi-intact preparation and *ex vivo* recording

Tissue preparation and *ex vivo* recording were performed as previously described (Choi et al., 2020; Hachisuka et al., 2016). Mice were anesthetized and the hair on the right hindpaw and hindlimb was clipped. After transcardial perfusion with oxygenated cold ACSF solution (in mM; 234 sucrose, 2.5 KCl, 0.5 CaCl<sub>2</sub>, 10 MgSO<sub>4</sub>, 1.25 NaH<sub>2</sub>PO<sub>4</sub>, 26 NaHCO<sub>3</sub>, 11 glucose), spinal cords (~C2 – S6) and hindlimbs were quickly excised and transferred into a dissection dish. Samples were incubated in a perfusion chamber (50 ml/min) with the same oxygenated ACSF. The skin innervated by the saphenous nerve were dissected away from surrounding tissues, without damaging the connection between L2/L3 DRGs to the spine and the nerves to the skin. After removing dura and pia membranes, spinal cords were pinned onto a Sylgard block with the right dorsal horn facing upward.

Recording was performed with continuous perfusion with oxygenated ACSF at 32°C. To visualize ErbB4+ (tdTomato+) cells in layers I/II, a narrow beam infrared LED (L850D-06 Marubeni, Tokyo, Japan, emission peak, 850 nm) was positioned near the solution surface. ErbB4+ cells were patched by a glass pipette filled with intracellular solution (in mM: 135 K-gluconate, 5 KCl, 0.5 CaCl<sub>2</sub>, 5 EGTA, 5 HEPES, 5 MgATP, pH 7.2) and recorded for APs in response to mechanical (firm brush) or thermal (50°C or 0°C saline) stimulations over the skin, to identify a receptive field. APs were recorded at different stimulation parameters: mechanical - 0.16 g, 1.0 g, 2.0 g and 4.0 g von Frey filaments and thermal - 0°C, 15°C, 40°C and 52°C saline by 10-ml syringe. AP frequency 10 sec ahead of stimulation was considered as baseline. After subtracting the baseline, cells with AP frequency larger than 2 Hz were considered as responders.

### Dorsal root stimulation

Activation of A $\beta$ , A $\delta$  and C fibers was performed as previously described (Baba et al., 1999; Duan et al., 2014). Dorsal root-attached sagittal spinal slices were prepared as aforementioned; dorsal roots were stimulated by placing a suction electrode at the dorsal root (about 12 mm from the entry) with increasing intensities at 0.05 Hz. EPSCs in ErbB4+ neurons were recorded to identify the smallest intensity that was able to elicit EPSCs. Such intensity was used as a guide to potential types of fibers ( $\leq 25$   $\mu$ A, 30–100  $\mu$ A, and 150–500  $\mu$ A for A $\beta$ , A $\delta$  and C fibers, respectively). Subsequently, ErbB4+ neurons would be recorded at 20 Hz for A $\beta$ , 2 Hz for A $\delta$ , and 1 Hz for C fibers; monosynaptic EPSCs were characterized by absence of synaptic failure and constant latency. Because high intensity stimulations may also activate A $\beta$  and A $\delta$  fibers, latencies of EPSC onsets were also characterized which verified respective inputs to ErbB4+ neurons (data not shown).

### Behavioral tests

Male mice 2~4 months old were used for behavioral tests. Prior to behavioral tests, animals were subjected to habituation, which consists of 3 trials of free exploration of the test apparatus, 30 min per day for 3 consecutive days.

To measure heat pain, mice were placed on a hot plate that was set at 52°C (Duan et al., 2014). They were monitored for the latency of foot lifting and licking. To avoid tissue damage, a cut-off time of 30 s was set.

To measure radiant heat pain, mice were exposed to Hargreaves test (Hargreaves et al., 1988). Mice were placed on a glass floor and covered with plexiglass chambers. Plantar surface of hind paws was stimulated by a beam of radiant heat (IITC Life Science) delivered from below the glass floor. Paw withdrawal was monitored. Light intensity that causes a latency of 8–12 s for control mice was used. A cut-off time of 20s was set to avoid tissue damage.

To measure capsaicin-induced foot licking, capsaicin (10  $\mu$ g in 10  $\mu$ l) was injected into the plantar surface of the right hind paw and time spent in licking the injected paw was measured for 5 min (Han et al., 2016).

To test the response to mechanical stimulation, mice were subjected to Von Frey test as previously described (Bonin et al., 2014; Dixon, 1965). They were placed on an elevated wire grid that was covered with plexiglass chambers. The center of plantar surface of the hind paw was stimulated with von Frey filament of different forces [0.02 g (#2) to 1.4 g (#9)]. Mice were monitored for paw withdrawal responses to identify lower-value filament for the next stimulation. If no response, a filament of higher value was used. A total of 5 stimulations were performed. The bending force (paw withdrawal threshold, PWT) was calculated with the following formula:  $PWT_{\text{force}} = 10^{(x \cdot F + B)}$ , in which  $x = 0.240$  and  $B = -2.00$ ,  $F$  is the calculated filament # value. In addition, mice were also tested for

paw withdrawal in response to sequential stimulation of plantar surface with filaments from 0.14 g to 1.4 g. Response percentage for each filament was calculated based on 10 times of stimulation.

To measure mechanical pain, we performed pinprick test and pinch test as previously described (Duan et al., 2014). Mice were placed on an elevated wire grid that was covered with plexiglass chambers. The center of plantar surface of the hind paw was stimulated with a 29-gauge needle attached to a 1-gram von Frey filament. Mice were monitored for withdrawal response out of 10 times of stimulation (with 1 min inter-stimulation intervals). In the pinch test, mice were monitored for the duration of foot licking in response to clamping of the skin of the hind paw by an alligator clasper. A 10-s cut-off time was set to avoid tissue damage.

To measure cold sensation, cold plate test and cold plantar assay were performed as previously described (Brenner et al., 2012; Duan et al., 2014). In cold plate test, mice were placed on a 0°C plate and the latency to paw flinching or licking were recorded. To avoid tissue damage, a 60-s cut-off time was set. In cold plantar assay, mice were placed on a ¼"-thick glass floor and the center of hindpaws were stimulated with a flattened dry ice pellet from beneath the floor. Time from onset of stimulation to paw withdrawal was recorded.

To measure cooling sensation, acetone evaporation assay was performed as previously described (Duan et al., 2014). Mice were placed on a mesh floor of a chamber. A drop of acetone was applied with a syringe to the mid plantar and the reaction was monitored and scored by 5 scales: 1, brief lift, flick, sniff, or startle; 2, paw shaking, jumping; 3, multiple lifts and licking; 4, prolonged lifting, licking, shaking, or jumping; 5, paw guarding.

To measure chemical itching response, calves were injected intradermally with chloroquine and histamine (200 and 100 µg, respectively in 10 µl PBS). Leg biting was recorded for 30 min.

To evaluate warm sensation, a two-choice temperature assay was performed (Pogorzala et al., 2013). Mice were placed on an apparatus with two plate surfaces (20 x 8 cm) that were at 30°C and variable 0~50°C, respectively. Mice were placed on one of the plates and allowed to freely explore the plates. The time spent in each chamber was monitored for 5 min.

### CFA and CCI models

Nerve injury were produced as previously described (Taves et al., 2016; Wang et al., 2020). Briefly, the common sciatic nerve of the left hindlimb was ligated (proximal to the trifurcation) with three sutures (1 mm apart). Ligatures were loosely tied until a subtle flick of the ipsilateral hind limb was observed. CFA (20 µl) was injected into the plantar of hindpaws unilaterally (Wang et al., 2020). Behavioral tests were performed 1 and 7 days after the procedure, respectively for CFA and CCI mice.

### Analysis of snRNA-seq data

Raw sequencing data (Russ et al., 2021) were downloaded from the NCBI database (accession code GSE158380) and processed with Cellranger. Dimensional reduction and clustering were performed with R package Seurat 4.0.0. Cells with transcripts less than 200 or more than 6000, >15% transcripts of mitochondrial genes or >5% hemoglobin genes were filtered out. Normalized expression values  $E_{i,j}$  for gene  $i$  in cell  $j$  were calculated by dividing unique molecular identifier (UMI) counts of gene  $i$  by the total UMI counts in cell  $j$ . To normalize the differences in coverage,  $E_{i,j}$  was multiplied by 10,000 to create transcript per million (TPM)-like values and  $\log_2(\text{TPM} + 1)$  were computed. Variable genes were identified using the FindVariableGenes method with the FastLogVMR dispersion function. The ScaleData function was used to scale and center the expression values in the dataset for dimensional reduction. Principal component analysis (PCA) was performed using Seurat functions based on the variable genes previously identified. PCs selected for further analysis were based on the examination of the contribution of each PC to overall variability and the contribution of genes to its PC. t-SNE was performed from selected PCs with the FindClusters function (resolution = 0.5). Marker genes for each cluster were determined via the FindAllMarkers function and compared with literature. FeaturePlot graph of ErbB4 was generated with the FeaturePlot function.

### QUANTIFICATION AND STATISTICAL ANALYSIS

Data analysis was performed with GraphPad Prism version 6.0. Unpaired Student's t-test (two-tailed) was used for comparison between two groups. Chi-squared test was used for the analysis of changes in responses to A $\beta$ , A $\delta$  and C stimulations. One-way ANOVA was used for analysis of the effects of NRG1 and afatinib on optically evoked EPSCs, followed by Sidak's multiple comparisons test. Gaussian distribution was analyzed with D'Agostino-Pearson normality test. Data were expressed as mean  $\pm$  SEM. n number in immunostaining, electrophysiology, and behavioral experiments refer to the number of analyzed slices, neurons, and animals, respectively.  $P < 0.05$  was considered significant. All data points were included in statistical analysis. To determine sample size, we followed previous similar experiments and used sample size calculator at ClinCalc.com (<http://clincalc.com/Stats/SampleSize.aspx>).